Documentation for Isotropic Finite Difference Time Domain Code

Peter R.T. Munro

October 5, 2025

Contents

1 Summary

This implementation of the Finite Difference Time Domain (FDTD) method is designed to model the scattering by isotropic materials including perfect dielectrics, lossy dielectrics and dispersive media. Reasonably general incident fields can be modelled, including plane waves and tightly focused fields[1]. The time dependence of the simulation can be either "pulsed" or "steady state". The FDTD grid must be a cuboid and all objects within it are modelled using a stair cased approximation. The sides of the Yee cell need not be of equal length however each Yee cell in the grid must be of identical dimensions. Multilayer structures with a profile uniform along one or two dimensions may be modelled. An understanding of much of the following will be enhanced by consulting the book by Taflove and Hagness [1].

[1]Practical restrictions are addresed in a later section

2 Introduction & Overview

2.1 Incident field

To be strictly correct the incident field should be introduced from the sides of a cuboid which surrounds the scattering regions. This is known as the "Total-Field/Scattered-Field" formulation. This implementation allows only for a steady-state simulation using this method. This involves slowly "ramping up" the inicident field and then waiting until the scattered-field reaches a steady state.

Tightly focused fields may be introduced by using a technique which is only strictly correct for waveguides. As long as "the majority" of the power in the incident field is contained within a single plane of the aforementioned cuboid, we can introduce the field from that plane only. This allows the use of the so-called pulsed mode where the incident field is introduced as a Gaussian modulated pulse. A time harmonic solution may be obtained by performing a discrete Fourier transform at the frequency of interest, normally the centre frequency of the Gaussian spectrum.

2.2 Materials

Materials comprising both the homogeneous background or multi-layer structure as well as the scattering cells may be specified using both the means of conductivity and relative permitivity or a dispersive model (Drude) may be used.

2.3 PML

A perfectly matched layer (PML) is implemented so that open scattering problems can be modelled. The PML correctly handles the case of dispersive and lossy materials as per Gedney [2, 3].

2.4 Field extraction

The time harmonic field can be obtained either at each point within the FDTD grid or on the surface of a cuboid. The latter is useful as it reduces

the copmutational and storage requirements whilst allowing the field outside the cuboid to be calculated using the Stratton-Chu integral [4, 5]. One however must ensure that all material inhomogeneities are contained within the cuboid and that only the scattered field is used in the Stratton-Chu calculation.

2.5 Performing a simulation

The software runs in a number of modes. It can be called directly from the Matlab command line or be called as a stand alone executable taking `.mat` files as input. Much of the internal details are hidden from the user and all inputs are specified from a text-based input file. The scattering cells are described using either a `.mat` file or a text file. The typical sequence for performing a simulation is as follows:

1. Specify simulation parameters for non-scattering cells in text input file.
2. Construct the scattering cell file.
3. Use the supplied m-file to either construct the program input file or to execute the simulation.
4. In the case that an input file is constructed in step 3, the simulation is executed.

3 Master input file specification

3.1 Introduction

The finite difference time domain (FDTD) method models the interaction of an incident electromagnetic field with a finite volume of space (denoted the computational space) composed of dielectric and conducting materials. The computational space is divided into cells each of which are identical in size. The material properties of each cell may differ however. Scattering objects may then be defined by varying the material composition of cells to model as closely as possible the geometry of the object to be modelled.

Many parameters must be set in order to specify a problem to be modelled. These parameters can be partitioned into a number of categories. For exam-

ple, the grid size and material composition must be specified. The properties of the source must also be specified. There are also a number of FDTD specific parameters that must also be set. The complete list of input parameter types is given below:

- Grid: These control the resolution and size of the grid as well as the default material in which scattering objects are embedded. Parameters to set the multilayer structure are included in this category.
- Source: These determine the properties of the incident electromagnetic field.
- Simulation type: Determines what kind of simulation is performed. Allows, for example, a simulation type amenable to analysis of the field in the time domain or the frequency domain to be chosen.
- FDTD specific: Parameters which are specific to the FDTD algorithm. These must be chosen by someone with some experience with FDTD. Some of the source parameters also fit into this category.
- Output: Determines which field parameters are calculated and outputed by the algorithm.
- Perfectly Matched Layer (PML): This is used to model unbounded free space scattering with a finite grid. These must be set by an experienced user.

A few concepts must be explained before outlining in detail the various input parameters. These relate to how the material composition of the grid is specified and also how the grid itself is indexed.

3.1.1 Grid indexing

In order to specify things like where the source field is introduced, where to extract the field and to specify grid material composition it is necessary to index the FDTD grid. This is done in a logical way using a triple of indices (i, j, k) to specify the index of a cell along each axis. The only confusing factor is that sometimes a *interior* indexing scheme is used and sometimes a *global* indexing scheme is used.

In general the user need only worry about the interior indexing scheme and the global indexing scheme is used by the program internally. The two indexing schemes arise because of the previously mentioned perfectly matched layer. The perfectly matched layer is used to truncate the FDTD grid for open region scattering problems. It is a low reflection, high loss material for plane waves at any angle of incidence.

The thickness of the PML around the grid is set by an input parameter. Thus in many cases the first cell in the grid would be a PML cell. When specifying the problem to be modelled however, it is very inconvenient (and prone to error) for the user to worry about adding on the thickness of the PML to any index specified. Thus most indices used in the input file are given in the interior coordinate system which has its origin (cell $(1, 1, 1)$) as the first non-PML cell in the grid.

In some cases the global system may be used, for example, when the user wants to extract the calculate field in the PML (this would only seldomly be done however). When this is the case the user must explicitly state that the global system is being used. The global system has as its origin at the cell $(1, 1, 1)$ which is the first cell in the FDTD grid, PML or otherwise.

As an example, consider the FDTD grids depicted in Figure 1. In both cases an FDTD grid with 8 non-PML cells and a PML layer 2 cells thick on the lower plane of the grid in each dimension. The left set of axes illustrates the global coordinate system so the cell with index $(1, 1, 1)$ is the first cell in the grid. Notice also that the indices are all greater than or equal to 1. The right diagram illustrates the interior coordinate system. In this case the cell with index $(1, 1, 1)$ is in the interior of the grid and is at the first non-PML cell. Notice that indices may be less than 1 for this case.

3.2 Input File Format

The input file is written using the conventions of a matlab m-file. Thus, comments may be included using a %. A number of values *must* be specified in order for the FDTD program to execute. If a required value is not specified, the FDTD program will not execute but will report which value was not specified. The required input values are outlined below using the categories mentioned previously.

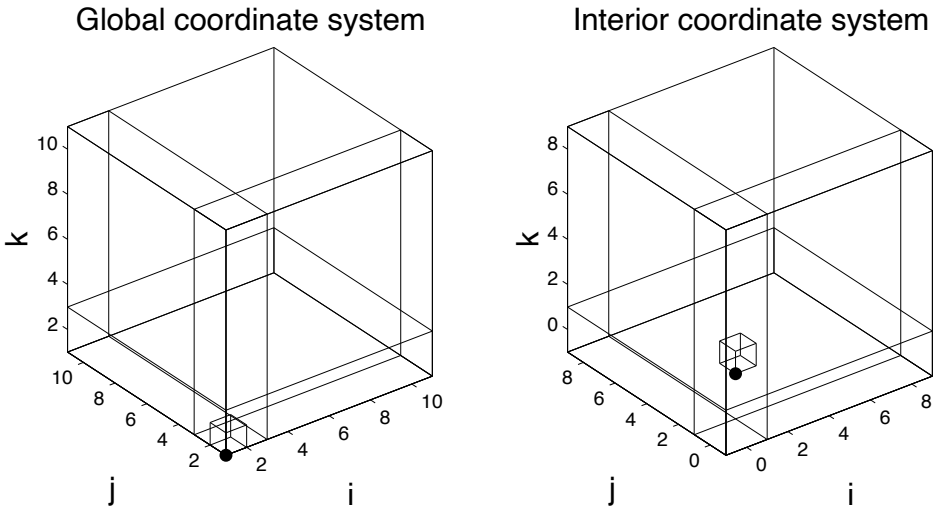

Figure 1: FDTD global and interior coordinate systems. A PML of layer 2 cells has been included on the lower side of the grid on each axis. The origin cell $(1, 1, 1)$ has been shown in each case

3.2.1 Grid

- `dimension`: This specifies the dimensionallity of the simulation. It can take the values `'TE'`, `'TM'` and `'3'` which represent the TE, TM and three dimensionaly simulations respectively. The default value of is `3` `dimension`
- `I`: The number of non-PML cells in the FDTD grid in the x-direction.
- `J`: The number of non-PML cells in the FDTD grid in the y-direction.
- `K`: The number of non-PML cells in the FDTD grid in the z-direction.
- `multilayer`: A double array of dimension $1 \times (N_l - 1)$ where N_l is the number of layers in the multilayer structure. Each element of `multilayer` gives the index of the Yee cell along the z-direction of an interface. A simulation without a multilayer structure, ie, homogeneous space would have `multilayer` set to `[]`. This is demonstrated in the example of Figure 2.
- `epsr`: A possibly complex vector of dimension $1 \times N_l$ representing the non-dispersive relative permitivity of the background material which may be a multilayer structure.

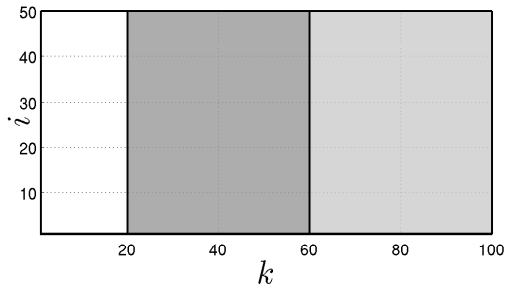

Figure 2: Diagram showing the layers in a multilayer structure for the case of `multilayer=[24 40]` and therefore $N_l = 3$.

- `wp_vec`: A vector of dimension $1 \times N_l$ which specifies the radian plasma frequency, ω_p, of each layer. See Section 4.1 for further details.
- `vc_vec`: A vector of dimension $1 \times N_l$ which specifies the collision frequency, ν_c, of each layer. See Section 4.1 for further details.
- `mur`: The relative permeability of the background material. All cells in the grid are assumed to be composed of this material unless specified otherwise in the materials file. This is generally not varied from unity.
- `structure`: A $2 \times N$ matrix specifying the piece-wise linear profile of the multilayer structure when looking at the xz profile. Suppose that `structure` and `multilayer` are defined as:

  ```
  structure = [i1 i2 ... iN;dk1 dk2 ... dkN];
  multilayer = [ki];
  ```

  then instead of having a plane interface at lattice coordinate $k1$, there is instead a piece-wise linear interface with vertices $(i1, ki+dk1)$, $(i2, ki+dk2)$, ..., $(iN, ki+dkN)$. Note that the structure is uniform along the j direction of the lattice.
- `delta`: *This should be set by someone with experience with FDTD and tested for suitability.* Describes the FDTD cell widths, must be a a matlab struct with the following members:
  - `delta.x`: Width of each FDTD cell in the x-direction (in m).
  - `delta.y`: Width of each FDTD cell in the y-direction (in m).

- `delta.z`: Width of each FDTD cell in the z-direction (in m).

- `material_file`: This is the name of the file which describes the scattering object within the FDTD grid. This is explained in more detail in the accompanying "FDTD material composition input file" document. This is most often specified at the time calling the setup function in order to avoid having a large number of input files.

3.2.2 Source

- `f_an`: The frequency in Hz of the incident electromagnetic field. This is the centre frequency of the source since the source is in general modulated by a Gaussian pulse.

- `interface`: Describes where the incident field is introduced into the grid. Must be a matlab struct with the following members:

  - `interface.I0`: A 1×2 vector where the first element gives the index i of a plane parallel to the jk plane where the incident field is introduced. The second element of the vector is a boolean value which determines whether or not the field will be introduced at the specified plane. The field will not be introduced if this is set to 0.

  - `interface.I1`: A 1×2 vector where the first element gives the index i of a plane parallel to the jk plane where the incident field is introduced. The second element of the vector is a boolean value which determines whether or not the field will be intrduced at the specified plane. The field will not be introduced if this is set to 0.

  - `interface.J0`: A 1×2 vector where the first element gives the index j of a plane parallel to the ik plane where the incident field is introduced. The second element of the vector is a boolean value which determines whether or not the field will be intrduced at the specified plane. The field will not be introduced if this is set to 0.

  - `interface.J1`: A 1×2 vector where the first element gives the index j of a plane parallel to the ik plane where the incident field is introduced. The second element of the vector is a boolean value which determines whether or not the field will be intrduced at the specified plane. The field will not be introduced if this is set to 0.

  - `interface.K0`: A 1×2 vector where the first element gives the index k of a plane parallel to the ij plane where the incident field

is introduced. The second element of the vector is a boolean value which determines whether or not the field will be intrduced at the specified plane. The field will not be introduced if this is set to 0.

- `interface.K1` A 1×2 vector where the first element gives the index k of a plane parallel to the ij plane where the incident field is introduced. The second element of the vector is a boolean value which determines whether or not the field will be intrduced at the specified plane. The field will not be introduced if this is set to 0.

Six interface vectors are specified so that the incident field can be introduced on the surface of a cuboid. Inside the cuboid the total field is calculated and outside the cuboid the scattered field is calculate. Note that in most cases that we currently consider, *only interface.K0 is required, the other interface conditions will be ignored.* A diagram of a typical configuration is shown in Figure 3. The PML layers around the outer boundary have been included along with the interface plane. As shown in the right diagram (where some PML layers have been cut away), the interface plane marks the boundary between total and scattered field regions. The scattered field can always be recovered from the total field by subtracting the incident field from the total field.

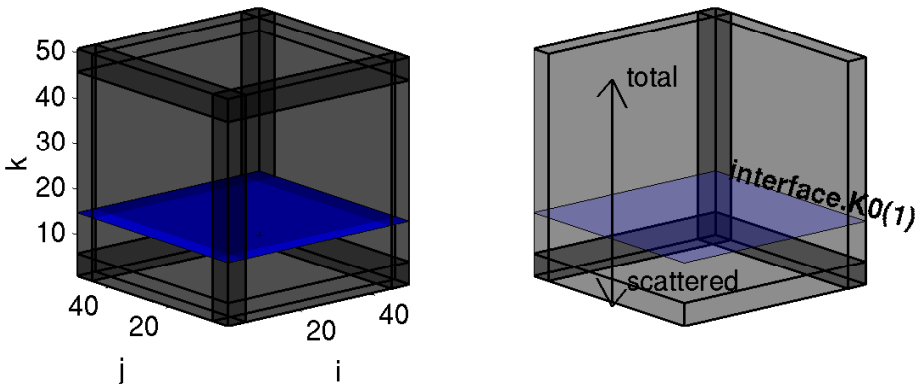

Figure 3: Diagram of FDTD grid showing the PML and the interface plane. The right diagram the is same as the left except 3 of the PML layers have been cut away for clarity. The interface plane has been made partially transparent for clarity also.

- `efname`: The name of the m-file (as a string) which describes the incident electric field. The function should be structured as (where for

example the line `efname = 'plane_wave_electric'` appears in the input file):

```
function [E] = plane_wave_electric(X,Y,Z)
```

Where:

- the parameters `X`,`Y` and `Z` will be 2-dimensional arrays similar in structure to that which may be obtained by a call to matlab's `meshgrid` function. Note however that it should not be assumed that `meshgrid` has been employed. Values are passed with units of m.
- `E` is a 1×3 cell array where `E{1}` contains the x-components of electric field, `E{2}` contains the y-components of electric field and `E{3}` contains the z-components of electric field.

Note that following relationship between the inputs `X`,`Y` and `Z` and the output `E` must hold:

$$\begin{aligned} E\{1\}(i,j) &= E_x(X(i,j), Y(i,j), Z(i,j)) \\ E\{2\}(i,j) &= E_y(X(i,j), Y(i,j), Z(i,j)) \\ E\{3\}(i,j) &= E_z(X(i,j), Y(i,j), Z(i,j)) \end{aligned}$$

Also note that the field should obey the $\exp(-\imath\omega t)$ *convention.*

- `hfname`: The name of the m-file (as a string) which describes the incident magnetic field. This should have structure idential to that of the electric field function described above. *Also note that the field should obey the* $\exp(-\imath\omega t)$ *convention.*
- `illorigin`: Defines the cell which fixes the origin of the cartesian coordinate system of the FDTD grid. The incident electromagnetic field is defined relative to this coordinate system. For more information on this, see the section titled "Compuational space coordinate system" in the accompanying "FDTD material composition input file" document.
- `z_launch`: Sets the z-coordinate of the `illorigin` cell. This cell will then have a position of $(0, 0, z\_launch)$ in the cartesian coordinate system of the grid. The cartesian coordinates of other cells are found using

the width of each FDTD cell. The cartesian coordinates are mapped to the interior FDTD lattice indices according to:

$$\begin{bmatrix} x \\ y \\ z \end{bmatrix} = \begin{bmatrix} \Delta x & 0 & 0 \\ 0 & \Delta y & 0 \\ 0 & 0 & \Delta z \end{bmatrix} \begin{bmatrix} i - O_x \\ j - O_y \\ k - O_z \end{bmatrix} + \begin{bmatrix} 0 \\ 0 \\ z_{launch} \end{bmatrix} \quad (1)$$

where `illorigin`= $[O_x, O_y, O_z]$, `z_launch`= z_{launch} and `delta.x`= Δx and so on for the other components.

- `wavelengthwidth`: *This parameter should be set by someone with experience in FDTD and should always be tested for suitability.* This is the spectral width of the modulating pulse of the incident electromagnetic field. The spectral width of this pulse should not be too wide as this will lead to the grid being unable to sufficiently spatially sample the field.

3.2.3 Simulation type

- `sourcemode`: Specifies the type of source being employed. This may take the value `'pulsed'` or `'steadystate'`. These options have the following meaning:
  - `'pulsed'`: This is the most commonly used method. It means that the incident electromagnetic field is introduced at a plane given by $k = interface.K0(1)$ and is introduced as a Gaussian pulse. A steady state response is calculated by taking a discrete Fourier transform at the required centre frequency (ie, that of the source) and accounting for the Fourier spectrum of the modulating pulse.
  - `'steadystate'`: This is when the incident electromagnetic field is gradually introduced and iteration continues until a steady state has been reached. When this option is used, the field around all faces of the interface cuboid must be specified (see section 3.2.2).
- `runmode`: This can take two values, `'complete'` or `'analyse'`. These have the following meaning:
  - `'complete'`: Means the simulation will be run and phasors extracted and no time resolved information can be obtained from the simulation. This is the most common option. Note that this option must be used when the simulation is being run as a stand alone application (rather than being run from matlab).

– `'analyse'`: Means the simulation will be run and the field at each iteration may be output to a file. This is useful for debugging or where it may be useful to view the field as it evolves in time. This option may only be used when the simulation is being run from matlab and not when it is being run as a stand alone application.

3.2.4 FDTD specific

These parameters should be set by an experienced FDTD user as they have a significant effect upon the accuracy of the simulation.

- `dt`: This is the time step parameter used by the FDTD simulation. This is subject to the restriction [1]:

$$dt \leq \frac{1}{c\sqrt{\frac{1}{delta.x^2} + \frac{1}{delta.y^2} + \frac{1}{delta.z^2}}} \tag{2}$$

  However the program will automatically alter this if necessary. As a general guide, the time step should be chosen to be close to the upper limit as this will lead to a lower number of iterations required to complete the simulation.

- `Nt`: The number of iterations to perform. This determines what period of time the FDTD simulates. Each iteration the FDTD simulation progresses by time `dt`. When a `'pulsed'` source is being used, the number of iterations must be set so that the field within the grid has decayed significantly. When a `'steadystate'` source is used the number of iterations must be dynamically set as a steady state must be reached before the simulation can end. In this case, `Nt` acts as an upper limit and the simulation will end if convergence is not reached.

3.2.5 Output

These options control how the results of the simulation are output.

- `outputs_array`: This enables various field components at selected points in the grid to be output at each iteration of the simulation. In general this should be set as `outputs_array={}` as this option

may only be used when `runmode` is set to `'analyse'`. Each element of the cell array is itself a cell array with the following structure: {filename,indextype,beginpoint,endpoint,components,writemethod} where:

  - **filename** is the name of the file or the base name used to write the data to.
  - **indextype** can take the value `'interior'` or `'global'` where in the former case the indices describing the range of cells to be output is given in interior coordinate system and in the latter case the global system is used (see Section 3.1.1).
  - **beginpoint** is a 1×3 vector of indices giving the coordinate in the FDTD lattice of one vertex of a cuboid within which the field is output.
  - **endpoint** is a 1×3 vector of indices giving the coordinate in the FDTD lattice of the vertex of a cuboid within which the field is output. Note that in general this is diagonally opposite the beginpoint when is cuboid is specified, however by making some members of beginpoint and endpoint equal, the field on planes and lines can be extracted.
  - **components** is a string containing one or more of the characters `'x'`,`'y'` and `'z'`. This is used to specify which field components are output.
  - **writemethod** can be either `'accumulate' or \verb`'dump'. In the former case a single mat file is written with all of the field data. In the latter case a separate fiel is written for each time increment.

- `exphasorsvolume`: Setting this to 1 will cause phasors in the entire volume of the FDTD grid (excluding the PML) to be calculated. This leads to significantly more memory to be used but often provides useful information.

- `exphasorssurface`: Setting this to 1 will cause phasors to be extracted about the surface of a user specified cuboid. This is the most memory efficient way to extract the field and is all that is necessary for the general imaging model.

- `phasorssurface`: Specifies the cuboid surface where the phasors should be extracted. Should be specified as:

```
phasorsurface = [i0 i1 j0 j1 k0 k1];
```

Where `i0` is one of the faces of the cuboid parallel to the jk plane in the grid. `i1` is the other face of the cuboid parallel to the jk plane in the grid. Note that `i0` should be less than `i1`. Similarly for the other indices. Figure 4 shows a sample mesh within an FDTD grid.

- `phasorinc`: Often the spacing of vertices on the surrounding surface need not be as close as the Yee cell dimension. In this case it may be possible, depending on the lattice dimension, to skip some vertices. `phasorinc` is thus a 1×3 dimensional vector of integers which divide their associated FDTD lattice dimension. That is, if `phasorinc=[pix,piy,piz]` then pix should divide I and piy should divide J etc. The default value of phasorinc is $[1, 1, 1]$.

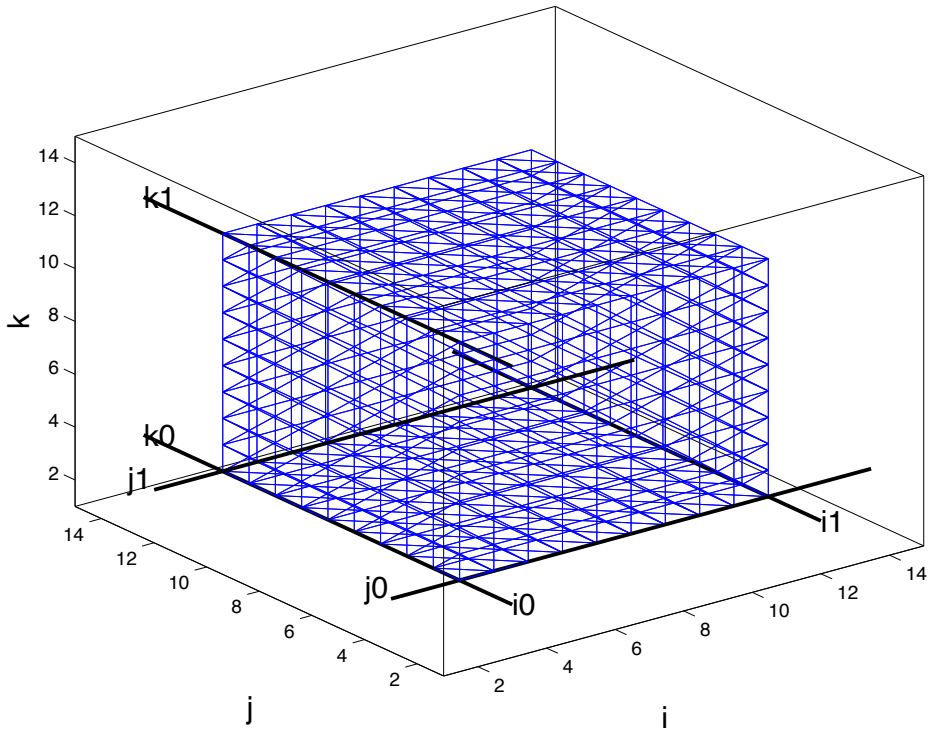

Figure 4: Sample mesh within the FDTD grid illustrating the meaning of i0 to k1.

3.2.6 PML

These parameters determine the properties of the PML. The PML is a layer of material which allows infinite scattering problems to be simulated using a finite grid. The PML acts as a very low reflection (theoretically zero), very high loss material. This any incident field is rapidly disipated with very small refelection. These should be set by an experienced user.

- `n`: The order of the PML. The conductivity of the PML is increased at a rate proporional to r^n where r is the depth iside the PML. This is to reduce reflection due to numerical discretisation. The value depends upon what type of material is being terminated. A value of 2 works well for dielectric materials however a higher value has been shown to be effective for conducting and dispersive materials [2, 3].

- `R0` This is the maximum reflectiviy for a plane wave of arbitrary incidence. A value of 10^{-5} is often used successfully here. This should be tested particularly for the termination conductive and dispersive media.

- `kappa_max`: When terminating conductive and dispersive materials it is necessary to have an additional parameter which varies with the same profile as the conductivity in the PML. It is set to 1 in the interior region. This maximum must be set through trial and error however Gedney has calculated some indicative values [2, 3]. In the case of terminating dielectrics this should be set to 1. Thus, `kappa_max` is an $1 \times N_i$ vector giving the value in each layer.

- `Dxl`: The thickness of the PML in the jk plane for cells having an i index lower than that of the first non-PML cell in the i-direction.

- `Dxu`: The thickness of the PML in the jk plane for cells having an i index greater than that of the last non-PML cell in the i-direction.

- `Dyl`: The thickness of the PML in the ik plane for cells having an j index lower than that of the first non-PML cell in the j-direction.

- `Dyu`: The thickness of the PML in the ik plane for cells having an j index greater than that of the last non-PML cell in the j-direction.

- `Dzl`: The thickness of the PML in the ij plane for cells having an k index lower than that of the first non-PML cell in the k-direction.

- `Dzu`: The thickness of the PML in the ij plane for cells having an k index greater than that of the last non-PML cell in the k-direction.

An example of how these variable relate to the PML widths is shown in Figure 5.

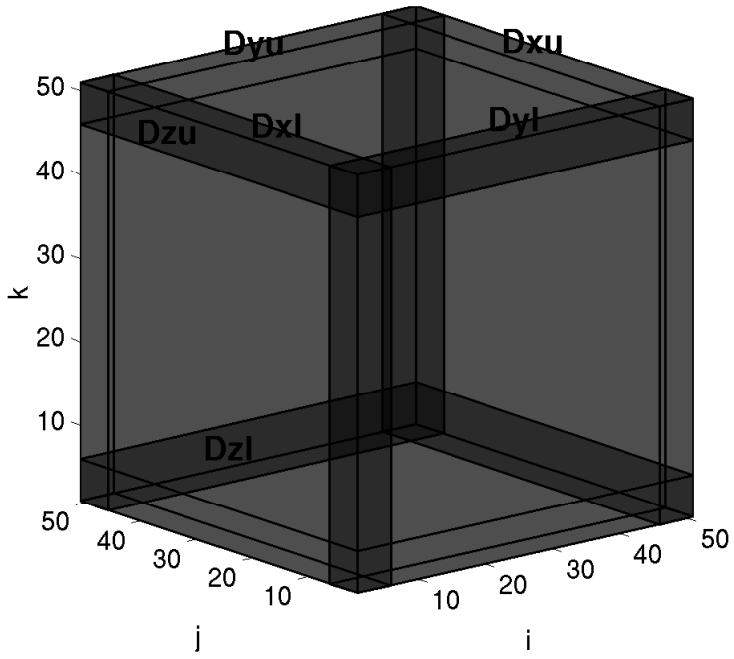

Figure 5: Example of how the variables Dxl to Dzu specify the PML widths.

4 Material file specification

The material file is used to specify the position and material type of scattering cells. Its definition draws heavily upon the mapping from the indexed space $\{(i,j,k)|1 \leq i \leq I, 1 \leq j \leq J, 1 \leq k \leq K\}$ to the cartesian space as defined by Eq. 1. The material file should be a `.mat` file with precisely two matrices named `material_matrix` and `composition_matrix`. `composition_matrix` is an $N \times 4$ array where N is the number of scattering cells. Each row of `composition_matrix` has the form:

$$\left[\text{ material\_id } \quad i \quad j \quad k \ \right] \tag{3}$$

where material_id is an integer denominating the type of material which makes up the scattering cell and is an index into the `material_matrix`. The triple (i, j, k) gives the position of the scattering cell represented by the matrix row. Each row of the `material_matrix` has the form:

$$\texttt{material\_matrix} = \left[\begin{array}{cccccccccccc} \text{material\_id} & \epsilon_r & \mu_r & \nu_c & \omega_p & \sigma_x & \sigma_y & \sigma_z & \sigma_x^* & \sigma_y^* & \sigma_z^* \end{array} \right] \tag{4}$$

where material_id is the integer identified of the material, ϵ_r is the real part of the relative permittivity and μ_r is the magnetic permeability. When using a dispersive material model ν_c is the collision fequency, ω_p is the radian plasma frequency. These should be set to 0 when not specifying a dispersive material. σ_x, σ_y, σ_z, σ_x^*, σ_y^* and σ_z^* are the conductivities associated with the split formulation of Berenger's [1]. In general, one should set $\sigma_x = \sigma_y = \sigma_z = \sigma$ to model a material with electrical conductivity σ.

4.1 Dispersive Media

Hitherto, we have not applied this model to the solution of time varying problems. Thus, unclusion of the Drude model is only to be able to model a general complex permitivity at a single frequency. Thus, it may be simpler to employ an expression the relative permitivity containing only a single pole however for a variety of reasons the full Drude model was implemented.

Starting with the definition of complex permitivity according to Drude and assuming the $\exp(-i\omega t)$ time convention:

$$\epsilon_r = \epsilon_\infty - \frac{\omega_p^2}{\omega\left(\omega + i\nu_c\right)} \tag{5}$$

where ω_p is the plasma frequency and ν_c is the collision frequency. We can establish the relationship between the refractive index and various terms in Eq. 5 according to:

$$\epsilon_r = (n_r + in_i)^2 \tag{6}$$

which yields:

$$\nu_c = \frac{2n_i n_r \omega}{\epsilon_\infty + n_i^2 - n_r^2} \tag{7}$$

$$\omega_p = \omega\sqrt{\epsilon_\infty + n_i^2 - n_r^2 + \frac{4n_i^2 n_r^2}{\epsilon_\infty + n_i^2 - n_r^2}} \tag{8}$$

These equations are sufficient to calculate ω_p and ν_c in order to obtain the desired relative permitivity at the radial frequency of interest ω. Tests with

the model suggest that a value of ϵ_∞ should be as close to unity as possible to obtain greater accuracy. The following section shows how the update equations in the non-PML part of the computational space are derived. More details can be obtained from Taflove and Hagness [1].

4.1.1 Derivation of update equations

Now we consider Ampere's law in the frequency domain:

$$\nabla \times \boldsymbol{H}(\omega) = \sigma \boldsymbol{E}(\omega) - i\omega\epsilon_0\epsilon_r(\omega)\boldsymbol{E}(\omega) \tag{9}$$

Inverse Fourier transform easily casts the first two terms of this equation into the time domain however the final term is somewhat more complex. This may however be done according to:

$$\begin{aligned} \mathfrak{F}^{-1}\left\{-i\omega\epsilon_0\epsilon_r(\omega)\boldsymbol{E}(\omega)\right\} &= \epsilon_0 \int_{-\infty}^{\infty} -i\omega \left(\epsilon_\infty - \frac{\omega_p^2}{\omega\left(\omega + i\nu_c\right)}\right) \boldsymbol{E}(\omega)\exp(-i\omega t)dt \\ &= \epsilon_0\epsilon_\infty \boldsymbol{E}'(t) + \boldsymbol{J}_p(t) \end{aligned} \tag{10, 11}$$

where

$$\int_{-\infty}^{\infty} \omega\left(\omega + i\nu_c\right)\boldsymbol{J}_p(\omega)\exp(-i\omega t)dt = \epsilon_0 \int_{-\infty}^{\infty} i\omega\omega_p^2 \boldsymbol{E}(\omega)\exp(-i\omega t)dt \tag{12}$$

the left side of this expression yields

$$\begin{aligned} \int_{-\infty}^{\infty} \omega\left(\omega + i\nu_c\right)\boldsymbol{J}_p(\omega)\exp(-i\omega t)dt &= \int_{-\infty}^{\infty} \left(\omega^2 + i\nu_c\omega\right)\boldsymbol{J}_p(\omega)\exp(-i\omega t)dt && (13) \\ &= \int_{-\infty}^{\infty} \left(-(-i\omega)^2 - \nu_c(-i\omega)\right)\boldsymbol{J}_p(\omega)\exp(-i\omega t)dt && (14) \\ &= -\boldsymbol{J}_p''(t) - \nu_c\boldsymbol{J}_p'(t) && (15) \end{aligned}$$

the right hand side of Eq. 12 yields

$$\epsilon_0 \int_{-\infty}^{\infty} i\omega\omega_p^2 \boldsymbol{E}(\omega)\exp(-i\omega t)dt = -\epsilon_0\omega_p^2\boldsymbol{E}'(t) \tag{16}$$

combining these results and eliminating the negative signs yields

$$\epsilon_0\omega_p^2\boldsymbol{E}'(t) = \boldsymbol{J}_p''(t) + \nu_c\boldsymbol{J}_p'(t) \tag{17}$$

this expresses a relationship between the electric field strength vector and an auxilliary quantity, the so-called polarisation current $J_p(t)$. We then express

Eq. 17 in terms of a discrete time step Δt using central differences. This is done by making the substitutions:

$$\epsilon_0 \omega_p^2 \left(\frac{\boldsymbol{E}^{n+1} - \boldsymbol{E}^{n-1}}{2\Delta t} \right) = \frac{\boldsymbol{J}_p^{n+1} - 2\boldsymbol{J}_p^n + \boldsymbol{J}_p^{n-1}}{\Delta t^2} + \nu_c \left(\frac{\boldsymbol{J}_p^{n+1} - \boldsymbol{J}_p^{n-1}}{2\Delta t} \right) \quad (18)$$

which results in the following update equation:

$$\boldsymbol{J}_p^{n+1} = \alpha \boldsymbol{J}_p^n + \beta \boldsymbol{J}_p^{n-1} + \gamma \left(\frac{\boldsymbol{E}^{n+1} - \boldsymbol{E}^{n-1}}{2\Delta t} \right) \quad (19)$$

where

$$\alpha = \frac{4}{\nu_c \Delta t + 2} \quad (20)$$

$$\beta = \frac{\nu_c \Delta t - 2}{\nu_c \Delta t + 2} \quad (21)$$

$$\gamma = \frac{2\epsilon_0 \omega_p^2 \Delta t^2}{\nu_c \Delta t + 2} \quad (22)$$

Returning to Eq. 9 we can write the time domain expression for Ampere's law as

$$\nabla \times \boldsymbol{H}(t) = \sigma \boldsymbol{E}(t) + \epsilon_0 \epsilon_\infty \boldsymbol{E}'(t) + \boldsymbol{J}_p(t) \quad (23)$$

before proceeding to discretise this equation we must make the observation that if $\boldsymbol{E}(t)$ is known at time step n then $\boldsymbol{H}(t)$ is known at time step $n + \frac{1}{2}$. Furthermore, $\boldsymbol{E}^{n+\frac{1}{2}}$ may be calculated according to $\boldsymbol{E}^{n+\frac{1}{2}} = \frac{1}{2}(\boldsymbol{E}^{n+1} + \boldsymbol{E}^n)$. We can then write:

$$\nabla \times \boldsymbol{H}^{n+\frac{1}{2}} = \sigma \frac{\boldsymbol{E}^{n+1} + \boldsymbol{E}^n}{2} + \epsilon_0 \epsilon_\infty \frac{\boldsymbol{E}^{n+1} - \boldsymbol{E}^n}{\Delta t} + \frac{\boldsymbol{J}_p^{n+1} + \boldsymbol{J}_p^n}{2} \quad (24)$$

$$= \sigma \frac{\boldsymbol{E}^{n+1} + \boldsymbol{E}^n}{2} + \epsilon_0 \epsilon_\infty \frac{\boldsymbol{E}^{n+1} - \boldsymbol{E}^n}{\Delta t} + \\ + \frac{1}{2} \left[(1+\alpha) \boldsymbol{J}_p^n + \beta \boldsymbol{J}_p^{n-1} + \frac{\gamma}{2\Delta t} \left(\boldsymbol{E}^{n+1} - \boldsymbol{E}^{n-1} \right) \right] \quad (25)$$

rearrangement of the equations yields the update equation for $\boldsymbol{E}^n$ as:

$$\boldsymbol{E}^{n+1} = C_a \boldsymbol{E}^n + C_c \boldsymbol{E}^{n-1} + C_b \Delta_i \left[\nabla \times \boldsymbol{H}^{n+\frac{1}{2}} - \frac{1}{2} \left((1+\alpha) \boldsymbol{J}_p^n + \beta \boldsymbol{J}_p^{n-1} \right) \right] \quad (26)$$

where Δ_i refers to the Yee cell width in cartesian direction i, being x, y or z.

$$\begin{aligned} C_a &= \frac{2\epsilon_\infty\epsilon_0 - \sigma\Delta t}{2\epsilon_\infty\epsilon_0 + \frac{1}{2}\gamma + \sigma\Delta t} \\ C_b &= \frac{1}{\Delta_i}\frac{2\Delta t}{2\epsilon_\infty\epsilon_0 + \frac{1}{2}\gamma + \sigma\Delta t} \\ C_c &= \frac{1}{2}\frac{\gamma}{2\epsilon_\infty\epsilon_0 + \frac{1}{2}\gamma + \sigma\Delta t} \end{aligned} \tag{27}$$

We now turn our attention to the discretisation of Eq. 26 in space. There is more than possible indexing scheme for the Yee cell. One such example is shown in Fig. 6. Under this indexing scheme, the field component E_x is located at position $(i+1/2, j, k)$ and similarly for the other field components. It is however simpler, and just as clear, to consider this field component as $E_x(i, j, k)$ and likewise for the other components. In this way the curl part

Figure 6: Diagram of a Yee cell showing how the various electromagnetic field components are sampled. The bolded cell shows the field components associated with cell (i, j, k).

of Eq. 26 is expanded as:

$$\begin{aligned} (\nabla \times \boldsymbol{H})_x &= \frac{1}{\Delta_y}(H_z(i,j,k) - H_z(i,j-1,k)) + \\ &\quad + \frac{1}{\Delta_z}(H_y(i,j,k-1) - H_y(i,j,k)) \end{aligned} \tag{28}$$

$$\begin{aligned} (\nabla \times \boldsymbol{H})_y &= \frac{1}{\Delta_z}(H_x(i,j,k) - H_x(i,j,k-1)) + \\ &\quad + \frac{1}{\Delta_x}(H_z(i-1,j,k) - H_z(i,j,k)) \end{aligned} \tag{29}$$

$$\begin{aligned} (\nabla \times \boldsymbol{H})_z &= \frac{1}{\Delta_x}(H_y(i,j,k) - H_y(i-1,j,k)) + \\ &\quad + \frac{1}{\Delta_y}(H_x(i,j-1,k) - H_x(i,j,k)) \end{aligned} \tag{30}$$

These equations thus permit the implementation of Eq. 26.

5 Output file format

The program writes the following variables into a `.mat` file:

```
Ex_out
Ey_out
Ez_out
Hx_out
Hy_out
Hz_out
x_out
y_out
z_out
Ex_i
Ey_i
Ez_i
Hx_i
Hy_i
Hz_i
x_i
y_i
z_i
vertices
camplitudes
facets
maxresfield
```

The meaning of each of these matrices is outlined below:

- `Ex_out`, `Ey_out`, `Ez_out`, `Hx_out`, `Hy_out` and `Hz_out` are complex amplitudes of the field defined within the non-PML FDTD lattice. Thus each field component is calculated at a different point in space as per the Yee cell. These are only calculated if `exphasorsvolume` is set to 1.
- `x_out`, `y_out`, `z_out` are the cartesian coordinates of the Yee cell origins of the fields specified in `Ex_out` etc. For example, the field component `Ex_out(i,j,k)` is associated with the Yee cell with origin positioned at (`x_out(i)`, `y_out(j)`, `z_out(k)`).
- `Ex_i`, `Ey_i`, `Ez_i`, `Hx_i`, `Hy_i` and `Hz_i` are complex amplitudes of the field defined at the same points in space by using interpolation.
- `x_i`, `y_i`, `z_i` are the cartesian coordinates of positions where the field components `Ex_i` etc are defined. For example, the field component `Ex_i(i,j,k)` is located at position (`x_i(i)`, `y_i(j)`, `z_i(k)`).

- `vertices` is an $N_v \times 3$ array of N_v vertices where the time harmonic field has been extracted. This is only calculated if `exphasorssurface` is set to 1.

- `camplitudes` is an $N_v \times 6$ array of complex amplitudes, one for each vertex. Each row of the array has the form $(E_x, E_y, E_z, H_x, H_y, H_z)$.

- `facets` is an $N_f \times 3$ array of integers such that each row defines a facet. The union of all facets describes a cuboid defined in `phasorsurface`. In general a mesh is represented by a set of vertices:

$$\mathrm{V} = \left\{ \mathbf{r}_{s,i} = \left(r^1_{s,i}, r^2_{s,i}, r^3_{s,i} \right) \in \mathbb{R}^3 | 1 \leq i \leq N_v \right\}$$

  a set of facets:

$$\mathrm{F} = \left\{ \left(v^1_i, v^2_i, v^3_i \right) \in \mathbb{N}^3, 1 \leq v^j_i \leq N_v, 1 \leq i \leq N_f \right\}$$

  where N_v is the number of vertices and N_f is the number of facets. The surface normal $\hat{\boldsymbol{n}}$ of facet i is given by:

$$\hat{\boldsymbol{n}} = \frac{(\mathbf{r}_{s,v^2_i} - \mathbf{r}_{s,v^1_i}) \times (\mathbf{r}_{s,v^3_i} - \mathbf{r}_{s,v^1_i})}{|(\mathbf{r}_{s,v^2_i} - \mathbf{r}_{s,v^1_i}) \times (\mathbf{r}_{s,v^3_i} - \mathbf{r}_{s,v^1_i})|}$$

  Note that this is an outward oriented surface normal.

- `maxresfield` is the maximum residual field in the FDTD lattice at the completion of the algorithm. This reveals whether a sufficient number of iterations have been executed in the case of a `pulsed` source.

6 Compiling the executeable

You will probably receive the files as a gzipped tar file which can be extracted as:

```
$gunzip dispersive1.2.tar.gz
$tar -xvf dispersive1.2.tar
```

A make file is defined at `dispersive/1.2/iterater/Makefile`. After setting the matlab root directory in the variable `MATLABROOT`, the following commands should be sufficient to compile the executeable code:

```
$make clean
$make
```

7 Running a simulation

7.1 Problem setup

The m-file `iteratefdtd_matrix` is used to setup or run the FDTD simulation. It has the following options:

```
iteratefdtd_matrix(input_file,operation,outfile,material_file,ill_file)

input_file    - file with input configuration information
operation     - either 'run', 'filesetup', 'gridsetup' or
'illsetup;. In the case of 'run', the FDTD
simulation is completed. In the case of
'filesetup', a mat file is written to file
outfile. In the case of 'gridsetup' only the FDTD
grid file is setup. In the case of 'illsetup' the illumination
matrices are calculated and saved in matfile given by outfile.
outfile       - the file that the above mentioned mat file is written to
material_file - the material may be specified as an argument or in the
input file. If it is specified by both, the one passed as a
function argument is used.
ill_file      - mat file containing the source field. Source will not
be computed if this string is non empty.
```

7.2 Problem execution

A simulation may be executed using one of a number of possibilities as outlined below:

```
Usage: openandorder [options] infile outfile
openandorder [options] infile gridfile outfile
Options:
```

```
-h:     Display this help message
-m:     Minimise output file size by not saving vertex and facet information
```

When a number of simulations are performed using the same simulation parameters with the exception of the scattering cells it is more efficient to specify the scattering cells seaprately in `gridfile`.

8 Examples

The samples are in the directory `dispersive1.2/doc/master/samples`.

8.1 Scattering of a plane wave by a dielectric sphere (case1)

This example calculates the light scattered by a sphere of refractive index 1.2 for an incident plane wave polarised in the y-direction. In order to create the input file, add `dispersive1.2` to the path. In particular, assuming the durrent directory is `dispersive1.2/doc/master/samples`, the directory may be added using the command `addpath('../../../');`. The input file, `input_file_sphere_case1.m` is listed below: the input `.mat` file is then created by calling `gen_input_sphere_case1` from the matlab prompt. This file is listed below: This results in the following output from matlab: This output shows that since this example does not use certain features which are available, and the inputs corresponding to these features have not been set, the m-file has set them to their default values. Also, note that two `.mat` files have been produced, one which is the actual scattering calculation and one which calculates the free space propagation of the incident wave. Note that although the incident wave is known analytically, the one which propagates in the FDTD computational space can very slightly due to numerical dispersion. The result of these scattering calculations are calculated according to:

```
$../../../iterater/prtmfdtd case1_fs.mat case1_fs_out.mat
$../../../iterater/prtmfdtd case1.mat case1_out.mat
```

Finally, the result can be compared to the field calculated using the series

of Mie by executing `analyse_res_case`, resulting in the results displayed in Figure .

Figure 7: Comparison between FDTD and Mie results for a dielectric sphere in air with relative permitivity 1.2. FDTD results are displayed on the top row.

The error may be calculated according to:

$$\epsilon_{\mathbf{E}}^{\mathbf{s}} = \frac{\sum_{i=1}^{N} |\mathbf{E}^{fdtd}(\mathbf{r}_i) \cdot \mathbf{s} - \mathbf{E}^{mie}(\mathbf{r}_i) \cdot \mathbf{s}|^2}{\sum_{i=1}^{N} |\mathbf{E}^{mie}(\mathbf{r}_i) \cdot \mathbf{s}|^2} \tag{31}$$

where N is the number of points where the field is sampled, $\mathbf{E}^{fdtd}$ is the field calculated using the FDTD method, $\mathbf{E}^{mie}$ is the field calculated using Mie theory, $\mathbf{r}_i$ is the position of the ith field value and $\mathbf{s}$ is the component of the field to consider. The error is calculated as:
note that $\epsilon_{\mathbf{H}}^{\hat{\mathbf{j}}}$ is not given as there is an error in calculating the y component

	$\hat{\mathbf{i}}$	$\hat{\mathbf{j}}$	$\hat{\mathbf{k}}$
E	0.0193	0.0194	0.0193
H	0.0194		0.0194

of the magnetic field.

8.2 Further examples of scattering of a plane wave by a sphere

Further examples have been constructed where the refractive index of the sphere is varied. There are examples where conductivity is used to obtain a complex refractive index and also where a dispersive model is used. Table summarises the properties of each example.

Each of these results can be analysed by setting the value of `sphere_case` in the m-file `analyse_res_case.m` and executing the m-file.

8.3 Reflection by a conducting medium

A further example is given where reflection of a plane wave by a plane conducting surface normal to the direction of propagation is calculated. The

m-file	n_{sphere}	model type	radius
`gen_input_sphere_case1.m`	1.2	dielectric	$\lambda/8$
`gen_input_sphere_case2.m`	1.2020 + 0.0701i	conductive	$\lambda/8$
`gen_input_sphere_case3.m`	1.2020 + 0.0701i	dispersive	$\lambda/8$
`gen_input_sphere_case4.m`	0.5020 + 4.9200i	dispersive	$\lambda/8$
`gen_input_sphere_case5.m`	0.5020 + 4.9200i	dispersive	$\lambda/4$

Table 1: Summary of sphere scattering examples.

input file is generated by the m-file
`dispersive1.2/doc/master/samples/multi_layer/gen_input_disp.m` and the result analysed by the m-file `calc_ref.m`.

8.4 Diffraction by a circular aperture

The m-file
`dispersive1.2/doc/master/samples/multi_layer/gen_input_ap.m` generates an input file which may be used to calculate the diffraction by a circular aperture in a conducting medium of finite thickness and conductivity.

References

[1] A. Taflove and S.C. Hagness. *Computational electrodynamics, second edition*. Artech House, 2000.

[2] S.D. Gedney. An anisotropic pml absorbing media for the fdtd simulation of fields in lossy and dispersive media. *Electromagnetics*, 16(4):399–415, 1996.

[3] S.D. Gedney. An anisotropic perfectly matched layer-absorbing medium for the truncation of fdtd lattices. *IEEE Trans. Ant. and Prop.*, 44(12):1630–1639, 1996.

[4] A.J. Poggio and E.K. Miller. *Computer techniques for electromagnetics*, chapter Integral equation solutions of three-dimensional scattering problems, pages 159–264. Pergamon Press, 1973.

[5] J. A. Stratton and L. J. Chu. Diffraction theory of electromagnetic waves. *Physical Review*, 56:99–107, 1939.

[6] S.K. Yee. Numerical solution of initial boundary value problems involving maxwell's equations in isotropic media. *IEEE Transactions on Antennas and Propagation*, 14(3):302–307, May 1966.

[7] A. Taflove and M.E. Brodwin. Numerical solution of steady-state electromagnetic scattering problems using the time-dependent maxwell's equations. *IEEE Transcactions on Microwave Theory and Techniques*, 23(8):623–630, August 1975.

[8] A. Taflove and M.E. Brodwin. Computation of the electromagnetic fields and induced temperatures within a model of the microwave-irradiated human eye. *IEEE Transactions on Microwave Theory and Techniques*, 23(11):888–896, November 1975.

[9] G. Mur. Absorbing boundary conditions for finite-difference approximation of the time-domain electromagnetic-field equations. *IEEE Transactions on Electromagnetic Compatibility*, 23(4):377–382, November 1981.

[10] J.-P. Berenger. A perfectly matched layer for the absorption of electromagnetic waves. *Journal of Computational Physics*, 114:185–200, 1994.

[11] K.S. Kunz and K.M. Lee. A three-dimensional finite-difference solution of the external response of an aircraft to a complex transient environment: Part i - the method and its application. *IEEE Transactions on Electromagnetic Compatibility*, 20(2):328–333, May 1978.

[12] A. Taflove. Application of the finite-difference time-domain method to sinusoidal steady-state electromagnetic-penetrations problems. *IEEE Transactions on Electromagnetic Compatibility*, 22(3):191–202, August 1980.

[13] D.M. Sullivan, O.P. Gandhi, and A. Taflove. Use of finite-difference time-domain method for calculating EM absorption in man models. *IEEE Transactions on Biomedical Engineering*, 35(3):179–186, March 1988.

[14] R.M. Joseph, Hagness S.C., and Taflove A. Direct time integration of maxwell's equations in linear dispersive media with absorption for scattering and propagations of femtosecond electromagnetic pulses. *Optics Letters*, 16(18):1412–1414, September 1991.

[15] R. Luebbers, F.P. Hunsberger, K.S. Kunz, R.B. Standler, and M. Schneider. A frequency-dependent finite-difference time-domain formulation fro dispersive materials. *IEEE Transcations on Electromagnetic Compatibility*, 32(3):222–227, August 1990.

[16] K. Umashankar and A. Taflove. A novel method to analyze electromagnetic scattering of complex objects. *IEEE Transactions on Electromagnetic Compatibility*, 24(4):397–405, 1982.

[17] A. Balyiss, M. Gunzburger, and E. Turkel. Boundayr conditions for the numerical solution of elliptic equations in exterior regions. *SIAM Journal on Applied Mathematics*, 42(2):430–451, April 1982.

[18] A. Bayliss and E. Turkel. Radiation boundary conditions for wave-like equations. *Communications in Pure and Applied Mathematics*, 23:707–725, 1980.

[19] R.L. Higdon. Numerical absorbing boundary conditions for the wave equation. *Mathematics of Computation*, 49(179):65–90, July 1987.

[20] R.L. Higdon. Absorbing boundary conditions for difference approximations to the multi-dimensional wave equation. *Mathematics of Computation*, 47(176):437–459, October 1986.

[21] B. Engquist. Absorbing boundary conditions for the numerical simulation of waves. *Mathematics of Computation*, 31(139):629–651, July 1977.

[22] Trefethen. L.N. and L. Halpern. Well-posedness of one-way wave equations and absorbing boundary conditions. *Mathematics of Computation*, 47(176):421–435, October 1986.

[23] J.-P. Berenger. Three-dimensional perfectly matched layer for the absorption of electromagnetic waves. *Journal of Computational Physics*, 127:363–379, 1996.

[24] R. Holland. Finite-difference time-domain (FDTD) analysis of magnetic diffusion. *IEEE Transactions on Electromagnetic Compatibility*, 36(1):32–39, February 1994.

[25] A. Taflove. *Computational Electrodynamics: The Finite Difference Time Domain Method*. Artech House, Boston and London, 1st edition, 1995.

[26] Z.S. Sacks, D.M. Kingsland, R. Lee, and J. Lee. A perfectly matched anisotropic absorber for use as an absorbing boundary condition. *IEEE Transactions on Antennas and Propagation*, 43(12):1460–1463, December 1995.

[27] J. Jin. *The finite element method of electromagnetics*. Wiley Interscience, 2002.

[28] J.D. Moerloose and M.A. Stuchly. Behavior of berenger's ABC for evanescent waves. *IEEE Microwave and Guided Wave Letters*, 5(10):344–346, Ocotber 1995.

[29] J.-P. Berenger. Evanescent waves in PMLs: Origin of the numerical reflection in wave-structure interaction problems. *IEEE Transactions on Antennas and Propagation*, 47(10):1497–1503, October 1999.

[30] J.-P. Berenger. Numerical reflection of evanescent waves by PMLs: origin and interpretation in the fdtd case. expected consequences to other finite methods. *International Journal of Numerical Modelling: Electronic Networks, Devices and Fields*, 13:103–114, 2000.

[31] C.W. Penney, R.J. Luebbers, and J.W. Schuster. Scattering from coated targets using a frequency-dependent, surface imperdance boundary condition in FDTD. *IEEE Transactions on Antennas and Propagation*, 44(4):434–443, April 1996.

[32] S. Van den Berghe, F. Olyslager, and D. De Zutter. Accurate modeling of thin conducting layers in FDTD. *IEEE Microwave and Guided Wave Letters*, 8(2):75–77, February 1998.

[33] R. Holland. Pitfalls of staircase meshing. *IEEE Transactions on Electromagnetic Compatibility*, 35(4):434–439, November 1993.

[34] S.A. Cummer. An analysis of new and existing FDTD methods for isotropic cold plasma and a method for improving their accuracy. *IEEE Transactions on Antennas and Propagation*, 45(3):392–400, March 1997.

[35] J.B. Judkins and R.W. Ziolkowski. Finite-difference time-domain modeling of nonperfectly conducting metallic thin-film gratings. *Journal of the Optical Society of America A*, 12(9):1974–1983, September 1995.

A The finite-difference time-domain method

A.1 Overview

The FDTD method differs appreciably from the methods discussed previously. All methods mentioned thus far are frequency domain methods and solve a boundary value problem. The FDTD method works in the time domain and solves an initial value problem. It literally models the evolution, over time, of a field incident upon a scatterer and the resulting scattered field. The method is attributed to Yee [6] who published the seminal paper on the FDTD method in 1966 although it was not applied in three dimensions until 1975 by Taflove [7, 8]. Since the publication of these papers, the method has developed immensely and is now a very mature numerical method used in numerous applications.

The starting point of the FDTD method is two of Maxwell's equations in the time domain:

$$\nabla \times \mathbf{E} = -\frac{\partial \mathbf{B}}{\partial t} - \sigma^* \mathbf{H} \tag{32}$$

$$\nabla \times \mathbf{H} = \mathbf{J} + \frac{\partial \mathbf{D}}{\partial t} \tag{33}$$

where σ^* is the equivalent magnetic loss (Ω/m) which is required in the analysis of PMLs. Each of these equations yields a set of coupled partial differential equations. For example, by using the constitutive relationships stated in Eq. (35):

$$\mathbf{D} = \epsilon_r \epsilon_0 \mathbf{E} \tag{34}$$

$$\mathbf{B} = \mu_r \mu_0 \mathbf{H} \tag{35}$$

where:
ϵ_r is the relative permittivity
ϵ_0 is the permittivity of free space
μ_r is the relative permeability, and
μ_0 is the permeability of free space

and also by making the substitution $\mathbf{J} = \mathbf{J}_{source} + \sigma \mathbf{E}$ where $\mathbf{J}_{source}$ represents a source of current density and σ is the material conductivity, the following partial differential equation is obtained from Eq. (33):

$$\frac{\partial E_x}{\partial t} = \frac{1}{\epsilon_r \epsilon_0} \left[\frac{\partial H_z}{\partial y} - \frac{\partial H_y}{\partial z} - (J_{source_x} + \sigma E_x) \right] \tag{36}$$

Yee's objective when developing the FDTD method was to discretise the coupled set of partial differential equations. Derivatives become differences during this process. One of the key features of the FDTD method is that it employs a central differencing scheme which achieves second order accuracy. To understand the concept of central differences, consider calculating the first derivative of a function $f(x)$ using only a difference equation. By expanding f in a Taylor series about x_i, it is possible to write:

$$f(x_i \pm \Delta x) = f(x_i) \pm \Delta x f'(x_i) + \frac{\Delta x^2}{2!} f''(x_i) \pm \frac{\Delta x^3}{3!} f'''(x_i) + \ldots \quad (37)$$

$$(38)$$

Subtracting $f(x_i - \Delta x)$ from $f(x_i + \Delta x)$ yields the following expression:

$$f(x_i + \Delta x) - f(x_i - \Delta x) = 2f'(x_i)\Delta x + \frac{2\Delta x^3}{3!} f'''(x_i) + \ldots \quad (39)$$

after dividing by $2\Delta x$, this gives $f'(x_i)$ as

$$f'(x_i) = \frac{f(x_i + \Delta x) - f(x_i - \Delta x)}{2\Delta x} + O(\Delta x^2) \quad (40)$$

This is called a central difference operation as the derivative of f may be approximated at a point which is in the centre of two points where the value of the function is known. The partial differential equations obtained from Maxwell's equations have both spatial and temporal derivatives. This means that special care must be taken when constructing the computational grid in order to facilitate spatial central differences and also when choosing the time stepping scheme to allow temporal central differencing. The FDTD simulation employs a regular grid of points where the various electromagnetic field components are sampled. The grid is built up through periodic replication of the Yee cell (see Fig. (9)). The position of a particular point within the grid is denoted by a triple of indices (i, j, k) which corresponds to position $(i\Delta_x, j\Delta_y, k\Delta_z)$ where Δ_x, Δ_y and Δ_z are the lengths of the Yee cell in the x, y- and z-directions respectively. Time is also discretised and referred to using a single increment n which corresponds to the simulation time $n\Delta t$ where Δt is the time increment being used in the simulation. Thus the x-component of the electric field at position $(i, j + 1/2, k + 1/2)$ and time $n - 1/2$ may be denoted by $E_x|^{n-1/2}_{i,j+1/2,k+1/2}\Delta t$.Using this notation, Eq. (36) may be written

as [1]:

$$\frac{E_x|^{n+1/2}_{i,j+1/2,k+1/2} - E_x|^{n-1/2}_{i,j+1/2,k+1/2}}{\Delta t} = \frac{1}{\epsilon_0 \epsilon_{r_{i,j+1/2,k+1/2}}} \begin{pmatrix} \frac{H_z|^n_{i,j+1,k+1/2} - H_z|^n_{i,j,k+1/2}}{\Delta y} - \\ \frac{H_y|^n_{i,j+1/2,k+1} - H_y|^n_{i,j+1/2,k}}{\Delta z} - \\ J_{source_x}|^n_{i,j+1/2,k+1/2} - \\ \sigma_{i,j+1/2k+1/2} E_x|^n_{i,j+1/2,k+1/2} \end{pmatrix} \tag{41}$$

It is noted from these equations that each E_x component must be positioned midway between two H_y and two H_z components. To proceed further a semi-implicit approximation must be used to replace the $E_x|^n_{i,j+1/2,k+1/2}$ term in Eq. (41) with:

$$E_x|^n_{i,j+1/2,k+1/2} = \frac{E_x|^{n+1/2}_{i,j+1/2,k+1/2} + E_x|^{n-1/2}_{i,j+1/2,k+1/2}}{2} \tag{42}$$

Resulting in the expression:

$$E_x|^{n+1/2}_{i,j+1/2,k+1/2} = C_a|_{i,j+1/2,k+1/2} E_x|^{n-1/2}_{i,j+1/2,k+1/2} + C_b|_{i,j+1/2,k+1/2} \begin{pmatrix} H_z|^n_{i,j+1,k+1/2} - H_z|^n_{i,j,k+1/2} + \\ H_y|^n_{i,j+1/2,k} - H_y|^n_{i,j+1/2,k+1} - \\ J_{source_x}|^n_{i,j+1/2,k+1/2} \Delta \end{pmatrix} \tag{43}$$

where C_a and C_b are functions of ϵ_r, σ, Δt, Δ and position within the FDTD grid and it is assumed that $\Delta x{=}\Delta y{=}\Delta z{=}\Delta$. Each of the partial differential equations like Eq. (36) may be converted into a difference equation in the same manner. The result of this is a system of equations where the **E** and **H** fields can be advanced by a time step at each iteration from an initial set of field values. Note that that in order to facilitate central differences in time, the **E** and **H** fields are calculated half a time step apart.

The difference equations also dictate a particular arrangement of field components within the computational grid proposed by Yee. The arrangement and the basic cell used to demonstrate this arrangement is known as the Yee cell and is shown in Fig. (9). It shows that the field components are offset from one another so as to allow the central difference equations to work correctly. Another important property of the Yee cell is its suitability to the application of PEC boundary conditions. On a PEC boundary the tangential component of electric field and normal component of magnetic field vanish.

Thus a PEC boundary is easily imposed upon any of the faces of the Yee cell.

As previously mentioned, the FDTD method essentially solves an initial value problem. In most problems however, a known field is incident upon the scattering object for a period comparable to the simulation time. In order to deal with this the FDTD grid is divided up into two regions. One region surrounds the scatterer and the total field is calculated in this region. Only the scattered field is calculated in the scattered region. This is very similar to the partitioning illustrated in Fig. (8). The incident field is introduced

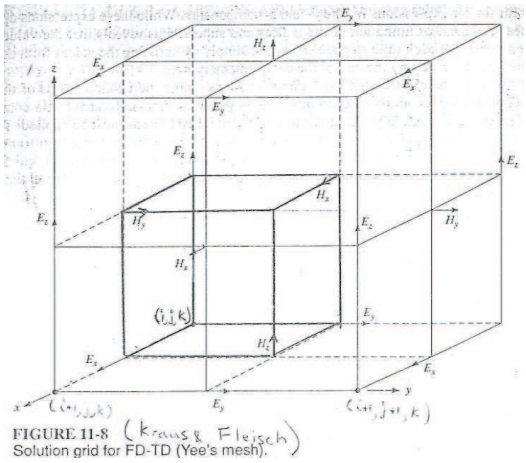

Figure 8: Diagram illustrating the partitioning of the computational space into two regions by the fictitious surface Γ_f. Only the scattered field is calculated in the shaded region whilst the total field is calculated in the interior region.

into the total field region by employing an additional update equation at the interface between the total and scattered regions. This update equation is actually required in order to maintain consistency between the scattered and total fields. In general, the interface between the total and scattered field is a box. Then by applying additional update equations on each face of the box, a plane wave of arbitrary propagation direction may be introduced to the total field region. This is however much more difficult for a more complex incident field such as a focused beam as there are so many plane wave components which make up the focused beam. The approximate solution to this problem is to introduce an interface plane which is extremely wide so that the focused field decays to nearly zero at its edges. This implies that the focused beam is incident through an aperture but by making the aperture large, its effect

is made insignificant. Mur [9] suggested the first kind of absorbing boundary condition however a number of other absorbing boundary conditions have since been suggested. The PML [10], as used in the FEM, is now the most widely used absorbing boundary condition. As previously explained, it is a layer of absorbing cells placed between the scatterer and the PEC boundary of the computational grid. The material content of the cells is especially designed such that the interface with the homogeneous region has a very low reflection.

A PML must be positioned in between the scatterer and the PEC boundary employed around the edge of the computational region. The PML was actually developed for use in the FDTD method by Berenger [10] however it was not the first absorbing boundary condition to be suggested. Mur [9] suggested the first kind of absorbing boundary condition however the PML has been shown to be the best performing absorbing boundary condition. The role of the PML is to absorb the the scattered field with minimal reflection. Details of how the PML works will are given in Sec. (B.7).

Since FDTD simulations are performed in the time domain, an additional step must be performed in order to extract the field in the frequency domain. One way of doing this is simply to wait until the fields reach a steady state within the computational region. When this method is employed, the incident field is introduced gradually and then maintained at a constant amplitude until a steady state is reached. Once steady state has been reached the time harmonic field may be extracted over the course of a few sinusoidal periods. Another method that may be employed is to modulate the incident field in time by Gaussian pulse but care must be taken to ensure that the pulse is sufficiently broad to restrict the bandwidth of the incident field. The field at various wavelengths may then be found through application of a discrete Fourier transform.

There are a few restrictions which must be observed in order for the FDTD method to work correctly. Firstly, the size of each Yee cell must be sufficiently small to accurately sample the field. This is usually of the order of $\lambda/20$ or smaller where λ is the centre wavelength of the incident illumination. There is also an upper bound on the time increment used by the method in order to guarantee stability of the simulation. In particular, in three dimensions, the time increment Δt must satisfy the Courant stability criterion [7]:

$$\Delta t \leq \frac{1}{c_{max}} \left(\frac{1}{\Delta x^2} + \frac{1}{\Delta y^2} + \frac{1}{\Delta z^2} \right)^{-1/2} \tag{44}$$

where c_{max} is the maximum wave phase velocity expected within the model.

The FDTD method uses memory in linear proportion to the number of cells within the computational grid thus making it relatively efficient compared with the MOM and the Green's tensor method. This however essentially implies that it uses memory in linear proportion to the number of scattering cells. This means that much larger scatterers can be modelled using the FDTD method than can be solved with the MOM and the Green's tensor method since as previously explained, these methods use memory in proportion with the square of the number of scattering cells.

Figure 9: Diagram of a Yee cell [6, 7] showing how the various electromagnetic field components are sampled.

The FDTD method has a number of advantages over other methods. The first advantage is that it is easy to implement. The simplicity stems from the very logical mapping of the algorithm into a computer program. Furthermore, the algorithm itself is rather simple. Because of the memory efficiency it is capable of modelling larger scatterers than the MOM and Green's tensor method and at least as big as that possible using the FEM. The FDTD method however does not suffer from the matrix inversion problem which plagues the FEM. It is in fact a very stable method. Another advantage is that the electric and magnetic fields are obtained simultaneously with equivalent accuracy. A final advantage of the FDTD method is that it is a very mature method. It has been applied to numerous applications [8, 11, 12, 13, 14] and so a great deal of knowledge has been acquired making the FDTD a very powerful tool the electromagnetic scattering calculations.

The FDTD method does of course have some non ideal attributes. To start with, it models dispersive materials poorly. This is because it is necessary to take a frequency domain description of a material and convert it to a time domain model. Numerous methods have been used (see [15] as an example) successfully however it must still be considered a weak point of the model. The regular orthogonal grid employed by the FDTD method is not suited to modelling complex objects. In general, the resolution of object features is limited to the grid cell size. Also, curved and sloping surfaces must be modelled by a stair case approximation. An example of the stair case approximation is shown in Fig. (10). The diagram shows how a pit used on an optical data storage disk is represented with increasingly fine stair case approximations. Only the FEM and MOM are able to avoid stair casing as they may employ an irregular mesh. Despite these disadvantages, the FDTD method is probably the most powerful method currently available for performing electromagnetic scattering calculations.

Figure 10: Diagram showing the top view of how a optical data storage pit is represented using a stair case approximation.

B Implementation details

B.1 Introduction

A brief account of the FDTD method is given in Sec. (A.1). This chapter contains a more comprehensive description of the method. It builds on concepts introduced in Sec. (A.1) and is intended to be largely self supporting.

B.2 Discretisation of Maxwell's equations

The principle behind the FDTD method is the discretisation in space and time of Maxwell's equations in differential form. Eqs. (32) and (33), repeated below for convenience:

$$\begin{aligned} \nabla \times \mathbf{E} &= -\frac{\partial \mathbf{B}}{\partial t} - \sigma^* \mathbf{H} \\ \nabla \times \mathbf{H} &= \mathbf{J} + \frac{\partial \mathbf{D}}{\partial t} \end{aligned}$$

In conjunction with the constitutive relations (Eqs. (34) and (35)) yield a set of coupled partial differential equations of the form:

$$\frac{\partial H_x}{\partial t} = \frac{1}{\mu_r \mu_0}\left[\frac{\partial E_y}{\partial z} - \frac{\partial E_z}{\partial y} - \sigma^* H_x\right] \tag{45}$$

$$\frac{\partial H_y}{\partial t} = \frac{1}{\mu_r \mu_0}\left[\frac{\partial E_z}{\partial x} - \frac{\partial E_x}{\partial z} - \sigma^* H_y\right] \tag{46}$$

$$\frac{\partial H_z}{\partial t} = \frac{1}{\mu_r \mu_0}\left[\frac{\partial E_x}{\partial y} - \frac{\partial E_y}{\partial x} - \sigma^* H_z\right] \tag{47}$$

$$\frac{\partial E_x}{\partial t} = \frac{1}{\epsilon_r \epsilon_0}\left[\frac{\partial H_z}{\partial y} - \frac{\partial H_y}{\partial z} - (J_{source_x} + \sigma E_x)\right] \tag{48}$$

$$\frac{\partial E_y}{\partial t} = \frac{1}{\epsilon_r \epsilon_0}\left[\frac{\partial H_x}{\partial z} - \frac{\partial H_z}{\partial x} - \left(J_{source_y} + \sigma E_y\right)\right] \tag{49}$$

$$\frac{\partial E_z}{\partial t} = \frac{1}{\epsilon_r \epsilon_0}\left[\frac{\partial H_y}{\partial x} - \frac{\partial H_x}{\partial y} - (J_{source_z} + \sigma E_z)\right] \tag{50}$$

where the substitution $\mathbf{J} = \mathbf{J}_{source} + \sigma \mathbf{E}$ has been made in order to represent both conduction currents ($\sigma \mathbf{E}$) and current sources ($\mathbf{J}_{source}$) within the com-

putational domain. In order to proceed, the computational volume must be partitioned into a number of cuboid cells as demonstrated in Fig. (11). Each field component is sampled once per cuboid cell in the manner suggested by Yee [6] and is shown in Fig. (9). Thus each cuboid shown in Fig. (11) contains a Yee cell. The position of field sample points within the computational volume is described by a set of indices (i, j, k) which correspond to position $(i\Delta_x, j\Delta_y, k\Delta_z)$ where Δ_x, Δ_y and Δ_z are the lengths of the Yee cell in the x-, y- and z-directions respectively. Thus the computational volume may be gridded with different resolution in each of the three orthogonal directions.

The arrangement of the Yee cell is important for two primary reasons. Firstly, it is ideal for imposing PEC boundary conditions on any face of the cell. This is because each face of the Yee cell contains components of electric field tangential to the face and a component of the magnetic field normal to the face. Thus a PEC boundary can be set on any face simply by setting these values to 0. Secondly, the field components are positioned such that central differences (see Sec. (A.1)) between components may be evaluated where they are required. For example, Eq. (45) involves the terms $\frac{\partial E_y}{\partial z}$ and $\frac{\partial E_z}{\partial y}$. Using Eq. (40) it becomes clear that in order to approximate these derivatives at a particular point in space using central differences, this point must be positioned in the middle of a line parallel to the z-axis joining two E_y sample points and on the middle of a line parallel to the y-axis joining two E_z sample points. This is precisely where the H_x sample point is located in the Yee cell, demonstrating why the Yee cell is arranged in the way that it is.

Figure 11: Gridding of computational volume into cuboid cells. A stair case approximation of a scatterer is indicated by the shaded cells.

Time must also be sampled. This is done by selecting a time step Δt which describes the spacing in time of successive samples in the simulation. In order to facilitate central differences in time, the magnetic and electric fields are calculated half a time step apart. Time within the simulation is denoted by an index n which corresponds to time $n\Delta t$. Using this system of indexing space and time, field components are indexed as, for example, $E_x|^{n+1/2}_{i,j+1/2,k+1/2}$ which denotes the value of E_x at time $t = (n+1/2)\Delta t$ and position $(i\Delta_x, (j+1/2)\Delta_y, (k+1/2)\Delta_z)$. The diagram in Fig. (13) shows that if the Yee cell is centred on position (i, j, k) then the E_x component is indeed located at $(i, j+1/2, k+1/2)$.

By employing this sampling scheme in space and time and approximating

each derivative in Eqs. (45) to (50) with a central difference operation (see Sec. (A.1)), the following set of difference equations is obtained after some manipulations [1]:

$$\begin{aligned} E_x|^{n+1/2}_{i,j+1/2,k+1/2} =& C_a|_{i,j+1/2,k+1/2} E_x|^{n-1/2}_{i,j+1/2,k+1/2} + \\ & C_{b_y}|_{i,j+1/2,k+1/2} \left(H_z|^n_{i,j+1,k+1/2} - H_z|^n_{i,j,k+1/2} \right) + \\ & C_{b_z}|_{i,j+1/2,k+1/2} \left(H_y|^n_{i,j+1/2,k} - H_y|^n_{i,j+1/2,k+1} \right) - \\ & C_{b_x}|_{i,j+1/2,k+1/2} J_{source_x}|^n_{i,j+1/2,k+1/2} \Delta_x \end{aligned} \tag{51}$$

$$\begin{aligned} E_y|^{n+1/2}_{i-1/2,j+1,k+1/2} =& C_a|_{i-1/2,j+1,k+1/2} E_y|^{n-1/2}_{i-1/2,j+1,k+1/2} + \\ & C_{b_z}|_{i-1/2,j+1,k+1/2} \left(H_x|^n_{i-1/2,j+1,k+1} - H_x|^n_{i-1/2,j+1,k} \right) + \\ & C_{b_x}|_{i-1/2,j+1,k+1/2} \left(H_z|^n_{i-1,j+1,k+1/2} - H_z|^n_{i,j+1,k+1/2} \right) - \\ & C_{b_y}|_{i-1/2,j+1,k+1/2} J_{source_y}|^n_{i-1/2,j+1,k+1/2} \Delta_y \end{aligned} \tag{52}$$

$$\begin{aligned} E_z|^{n+1/2}_{i-1/2,j+1/2,k+1} =& C_a|_{i-1/2,j+1/2,k+1} E_z|^{n-1/2}_{i-1/2,j+1/2,k+1} + \\ & C_{b_x}|_{i-1/2,j+1/2,k+1} \left(H_y|^n_{i,j+1/2,k+1} - H_y|^n_{i-1,j+1/2,k+1} \right) + \\ & C_{b_y}|_{i-1/2,j+1/2,k+1} \left(H_x|^n_{i-1/2,j,k+1} - H_x|^n_{i-1/2,j+1,k+1} \right) - \\ & C_{b_z}|_{i-1/2,j+1/2,k+1} J_{source_z}|^n_{i-1/2,j+1/2,k+1} \Delta_z \end{aligned} \tag{53}$$

$$\begin{aligned} H_x|^{n+1}_{i-1/2,j+1,k+1} =& D_a|_{i-1/2,j+1,k+1} H_x|^n_{i-1/2,j+1,k+1} + \\ & D_{b_z}|_{i-1/2,j+1,k+1} \left(E_y|^{n+1/2}_{i-1/2,j+1,k+3/2} - E_y|^{n+1/2}_{i-1/2,j+1,k+1/2} \right) + \\ & D_{b_y}|_{i-1/2,j+1,k+1} \left(E_z|^{n+1/2}_{i-1/2,j+1/2,k+1} - E_z|^{n+1/2}_{i-1/2,j+3/2,k+1} \right) \end{aligned} \tag{54}$$

$$\begin{aligned} H_y|^{n+1}_{i,j+1/2,k+1} =& D_a|_{i,j+1/2,k+1} H_y|^n_{i,j+1/2,k+1} + \\ & D_{b_x}|_{i,j+1/2,k+1} \left(E_z|^{n+1/2}_{i+1/2,j+1/2,k+1} - E_z|^{n+1/2}_{i-1/2,j+1/2,k+1} \right) + \\ & D_{b_z}|_{i,j+1/2,k+1} \left(E_x|^{n+1/2}_{i,j+1/2,k+1/2} - E_x|^{n+1/2}_{i,j+1/2,k+3/2} \right) \end{aligned} \tag{55}$$

$$\begin{aligned} H_z|^{n+1}_{i,j+1,k+1/2} =& D_a|_{i,j+1,k+1/2} H_z|^n_{i,j+1,k+1/2} + \\ & D_{b_y}|_{i,j+1,k+1/2} \left(E_x|^{n+1/2}_{i,j+3/2,k+1/2} - E_x|^{n+1/2}_{i,j+1/2,k+1/2} \right) + \\ & D_{b_x}|_{i,j+1,k+1/2} \left(E_y|^{n+1/2}_{i-1/2,j+1,k+1/2} - E_y|^{n+1/2}_{i+1/2,j+1,k+1/2} \right) \end{aligned} \tag{56}$$

where

$$C_a|_{i,j,k} = \left(1 - \frac{\sigma_{i,j,k}\Delta t}{2\epsilon_{r_{i,j,k}}\epsilon_0}\right) / \left(1 + \frac{\sigma_{i,j,k}\Delta t}{2\epsilon_{r_{i,j,k}}\epsilon_0}\right) \quad (57)$$

$$C_{b_s}|_{i,j,k} = \left(\frac{\Delta t}{\epsilon_{r_{i,j,k}}\epsilon_0\Delta_s}\right) / \left(1 + \frac{\sigma_{i,j,k}\Delta t}{2\epsilon_{r_{i,j,k}}\epsilon_0}\right) \quad (58)$$

$$D_a|_{i,j,k} = \left(1 - \frac{\sigma^*_{i,j,k}\Delta t}{2\mu_{r_{i,j,k}}\mu_0}\right) / \left(1 + \frac{\sigma^*_{i,j,k}\Delta t}{2\mu_{r_{i,j,k}}\mu_0}\right) \quad (59)$$

$$D_{b_s}|_{i,j,k} = \left(\frac{\Delta t}{\mu_{r_{i,j,k}}\mu_0\Delta_s}\right) / \left(1 + \frac{\sigma^*_{i,j,k}\Delta t}{2\mu_{r_{i,j,k}}\mu_0}\right) \quad (60)$$

and $\sigma_{i,j,k}$, $\sigma^*_{i,j,k}$, $\epsilon_{r_{i,j,k}}$ and $\mu_{r_{i,j,k}}$ are the conductivity, equivalent magnetic loss, relative permittivity and relative permeability respectively at grid location (i, j, k). s can be either of the orthogonal Cartesian axes labels x, y or z. Scatterers may thus be built up by specifying a distribution of the above parameters which depends upon grid position (i, j, k). Note that it is also necessary to make the so called semi-implicit approximation: $E_s|^n = (E_s|^{n+1/2} + E_s^{n-1/2})/2$ in order to treat the magnetic loss and conductivity terms appearing in Eqs. (45) to (50).

This system of difference equations provides a means by which, given $\mathbf{E}|^{n-1/2}$ and $\mathbf{H}|^n$ throughout the computational grid, $\mathbf{E}|^{n+1/2}$ may be found which may in turn be used, together with $\mathbf{H}|^n$ to calculate $\mathbf{H}|^{n+1}$. Thus, given an initial electromagnetic field throughout the entire computational volume, the electromagnetic field may be found at any later time subject to the time sampling scheme employed in the simulation. Note that this assumes the use of a boundary condition at the boundary of the computational region. This is dealt with in Sec. (B.7).

B.3 Introducing an incident waveform

Scattering problems typically have an incident illumination which gives rise to a scattered field. The method most commonly employed to introduce an incident wave into a simulation is called the Total Field/Scattered Field (TF/SF) formulation [9, 16]. This method works by partitioning the computational region into two volumes as shown in Fig. (12). The linearity of Maxwell's equations permits the total electromagnetic field to be decomposed as:

$$(\mathbf{E}, \mathbf{H}) = (\mathbf{E}^i, \mathbf{H}^i) + (\mathbf{E}^s, \mathbf{H}^s)$$

where $(\mathbf{E}^i, \mathbf{H}^i)$ is the field due solely to the incident field in the absence of a scatterer and is generally known analytically. The scattered field $(\mathbf{E}^s, \mathbf{H}^s)$ is the difference between the total field actually present and the incident field. $(\mathbf{E}^i, \mathbf{H}^i)$ and $(\mathbf{E}, \mathbf{H})$ must satisfy Maxwell's equations in the homogeneous space surrounding the scatterer and as a result so must $(\mathbf{E}^s, \mathbf{H}^s)$. Inside the scatterer, $(\mathbf{E}^s, \mathbf{H}^s)$ should be considered the perturbation to the incident field to ensure that the total field satisfies Maxwell's equations. It should be stressed that this representation is not an approximation, simply a convenient decomposition of the field. To demonstrate how the incident waveform is

Figure 12: Diagram showing the partitioning the computational volume into total field and scattered field regions separated by the fictitious surface Γ_f.

introduced consider the example depicted in Fig. (13). The shaded plane through the Yee cell centre marks the boundary between the scattered and total field regions. The scattered field is stored for values of y less than where the boundary is positioned and the total field is stored elsewhere. Consider the update equation for $\mathrm{H}_{z,1}$, given by Eq. (56). It is incorrect to apply this equation, without modification, to update $\mathrm{H}_{z,1}$ as the update equation would contain terms which are from the scattered field region and some which are from the total field region. The incident field is however generally known analytically and so the update equation for $\mathrm{H}_{z,1}$ may be written as:

$$\begin{aligned} H_{z,1}|^{n+1} &= D_a H_{z,1}|^n + D_b \left(E_{x,2}|^{n+1/2} - \left(E^s_{x,1}|^{n+1/2} + E^i_{x,1}|^{n+1/2} \right) + \right. \\ &\quad \left. E_{y,1}|^{n+1/2} - E_{y,2}|^{n+1/2} \right) \\ &= D_a H_{z,1}|^n + D_b \left(E_{x,2}|^{n+1/2} - E^s_{x,1}|^{n+1/2} + E_{y,1}|^{n+1/2} - E_{y,2}|^{n+1/2} \right) - \\ &\quad D_b E^i_{x,1}|^n \end{aligned} \tag{61}$$

where it has been assumed that $\Delta_x = \Delta_y = \Delta$ and thus $D_{b_x} = D_{b_y}$. Eq. (61) implies that the FDTD algorithm may proceed as normal across the interface but an additional term, $D_b E^i_{x,1}|^n$, must be subtracted from the standard update equation in order to maintain consistency between the total and scattered regions. Similar equations for each update equation arise at each part of the cuboid boundary between the scattered and total fields. These may be viewed in Taflove and Hagness [1].

Figure 13: Diagram showing the boundary between scattered and total field regions and a Yee cell.

The temporal properties of the waveform to be introduced must be considered very carefully. For instance, if the time harmonic field of an incident wave is

known then it could be introduced simply by "switching on" the source at a particular time as if the source was modulated by a step function. This would however introduce high frequency components into the incident waveform which would degrade the accuracy of the simulation as the FDTD grid resolution is chosen so as to sample all spectral components adequately. This problem may be solved by gradually and smoothly increasing the amplitude of the incident waveform from 0 till the required amplitude is reached. This limits the introduction of high frequency components. The simulation is then allowed to proceed until a steady state is reached. The simulation must determine when steady state has been reached by comparing the field within the computational region over successive sinusoidal cycles. Extraction of the complex amplitude of the field phasors allow the time harmonic field to be extracted from the simulation.

An alternative to this method is to introduce an incident wave modulated by a single Gaussian pulse. The Gaussian pulse provides a way to accurately control the spectral width of the incident field. The time harmonic scattered field may then be found from the time domain scattered field by application of a Discrete Fourier Transform (DFT). When this method is used, the incident field in the time domain is given by:

$$\mathbf{E}^{inc}(\mathbf{r},t) = \Re\left\{ \imath\mathbf{E}_0 \exp(\imath(k_0\boldsymbol{\beta}\cdot\mathbf{r} - \omega_0(t-t_0))) \exp\left(-\pi\left(\frac{t-(t_0+\boldsymbol{\beta}\cdot\mathbf{r}/c)}{W_0}\right)^2\right)\right\} \tag{62}$$

where $\Re$ denotes the real part, $\mathbf{E}_0$ is the polarisation of the plane wave, ω_0 and k_0 are the angular frequency and wavenumber of the wave in the homogeneous region, $\boldsymbol{\beta}$ is the unit vector in the direction of propagation of the plane wave, W_0 controls the pulse width, t_0 controls the delay of the pulse peak, c is the speed of light in the homogeneous region and $\mathbf{r}$ is the position within the computational volume. Note that the factor of $\imath$ appears to ensure that the pulse has 0 DC content. W_0 must be chosen so that the spectral width of the incident waveform is sufficiently narrow and t_0 is chosen to ensure that the incident waveform starts with a vanishingly small amplitude. In particular, the spectral width of the modulating pulse may be analysed by taking the Fourier transform of $\exp(-\pi(t/W_0)^2)$ as:

$$\mathfrak{F}\left\{\exp(-\pi(t/W_0)^2)\right\} = W_0\exp(-\pi(fW_0)^2) \tag{63}$$

where $\mathfrak{F}$ is the Fourier transform operator. Then the spectral width of the incident waveform, Δf, defined as the Full Width at Half Maximum (FWHM) of $W_0\exp(-\pi(fW_0)^2)$ is given by $\Delta f = 2/W_0\sqrt{\log 2/\pi}$. The wavelength

width is however of more interest, which may be found using the relationships $f\lambda = c$ and $\Delta f \approx -c/\lambda^2 \Delta\lambda$ as $\Delta\lambda = 2\lambda^2/(cW_0)\sqrt{\log 2/\pi}$. Thus W_0 may be chosen to guarantee a particular $\Delta\lambda$. It is shown in a later section that a sufficient value of $\Delta\lambda/\lambda$ is of the order of 0.1. t_0 is set so that when the source starts at $t = 0$, it has a very small amplitude. Testing shows that an initial magnitude of 8 orders of magnitude below the peak amplitude is sufficient.

The time domain expression of the incident field, Eq. (62), is discretised as required by the FDTD update equations which maintain the consistency between scattered and total field regions. At each time step the incident field update equations are executed. The simulation must be run until the scattered field has decayed to many orders of magnitude lower than the peak scattered field. The time harmonic scattered field may then be found by application of a DFT to the time domain scattered field data. This may be done efficiently by considering the DFT of an arbitrary function $g(t)$ which may be considered as one of the field components. Then the DFT $G(f_0)$ is evaluated according to:

$$G(f_0) = \frac{1}{N} \sum_{k=0}^{N-1} g(k\Delta t) \exp(\imath 2\pi f_0 k \Delta t) \tag{64}$$

where N is the number of times $g(t)$ is sampled, Δt is the time between sample points and f_0 is the frequency at which the DFT is evaluated. Since the FDTD simulation steps through each of the indices $k = 0$ to $N - 1$, this sum is best evaluated incrementally as the simulation progresses. This avoids the need to store the complete time evolution of the scattered field which would be unfeasible. This is not the end of the story as the frequency spectrum of the incident field must be taken into account. This is most conveniently done by calculating the DFT of the modulating pulse concurrently with the field DFT. The time harmonic scattered field at a particular frequency may then be found by dividing the DFT of the field by the DFT of the modulating pulse at the frequency of interest.

This method of introducing an incident field using a pulsed excitation is preferred since it avoids the problem of establishing when the field reaches a steady state. Also, as an added bonus, it allows the broadband response of a structure to be calculated based upon a single FDTD simulation.

The incident wave theory represented hitherto is valid only for a single plane wave excitation. This is because a particular direction of propagation of the wave front must be chosen in order that the amplitude of the modulating

pulse may be calculated at the boundary between the total and scattered field regions. Thus one way of modelling a complex incident waveform is to decompose it into an angular spectrum representation. An FDTD simulation would then need to be carried out for each plane wave component or multiple update equations would need to be applied at the boundary between total and scattered field, one for each plane wave component. Both of these methods are computationally demanding. Fortunately there is an approximation which may be used in the case where the incident wave is a focused beam.

In the vicinity of the focus of a high NA lens, the field decays extremely quickly in the transverse direction. Thus it is possible to define a window transverse to the optical axis of the lens, positioned near the focus of the lens such that most of the energy of the beam propagates through the window. Thus the field at the edges of the window are vanishingly small. When this is the case it is possible to neglect the update equations on the edges of the window. This allows a complex waveform to be launched into the computational volume with minimum computational load.

This approximation may be interpreted in a number of ways. Firstly it may be considered that the focused beam is apertured. Since the aperture is large compared to the focused spot it has a negligible effect. Secondly, this is very similar to the way waveguides are modelled using the FDTD method. If the field were being launched into a waveguide it would be completely valid. The validity of this approximation will be considered in Sec. (B.9.1).

B.4 Numerical dispersion

Ideally, the phase velocity of a plane wave propagating within a homogeneous FDTD computational volume is determined entirely by the material properties of the computational volume. This is not the case. The FDTD method introduces what is known as numerical dispersion into the obtained solution. This arises because the grid size and time step place a constraint on the phase velocity of waves travelling in the FDTD system. A full analysis of numerical dispersion is beyond the scope of this section however it is possible to obtain some results for restricted cases.

The strategy is as outlined by Taflove [1] and involves postulating a trial solution for a plane wave propagating within a FDTD simulation. The solution obtained at an arbitrary time step using the FDTD method is equated with the analytic solution of the wave being launched into the system. The resulting system of equations permits the relationship between phase velocity,

grid size and time step to be established. The relationship given by Taflove [1] for a plane wave propagating in a three dimensional Yee grid is:

$$\left[\frac{1}{c\Delta t}\sin\left(\frac{\omega\Delta t}{2}\right)\right]^2 = \left[\frac{1}{\Delta_x}\sin\left(\frac{\tilde{k}_x\Delta_x}{2}\right)\right]^2 + \left[\frac{1}{\Delta_y}\sin\left(\frac{\tilde{k}_y\Delta_y}{2}\right)\right]^2 + \left[\frac{1}{\Delta_z}\sin\left(\frac{\tilde{k}_z\Delta_z}{2}\right)\right]^2 \quad (65)$$

where ω is the angular frequency of the numerical wave and $\tilde{k} = (\tilde{k}_x, \tilde{k}_y, \tilde{k}_z)$ is the wave vector of the numerical wave. This relationship is too complex to analyse in three dimensions and so the problem is reduced to two dimensions by selecting $k_z = 0$. Then a numerical wave propagating at an angle ϕ to the x-axis of the numerical grid with $\Delta = \Delta_x = \Delta_y$ is postulated. This results in the following dispersion relation:

$$\frac{1}{S^2}\sin^2\left(\frac{\pi S}{N_\lambda}\right) = \sin^2\left(\frac{\Delta\tilde{k}\cos\phi}{2}\right) + \sin^2\left(\frac{\Delta\tilde{k}\sin\phi}{2}\right) \quad (66)$$

where S is the Courant number defined as $S = c\Delta t/\Delta$ and N_λ is the grid sampling density defined as $N_\lambda = \lambda_0/\Delta$ where λ_0 is the wavelength of the numerical wave. The objective is to solve for $\tilde{k}$ given S, N_λ, Δ and ϕ. This cannot be done easily in general and a numerical method, such as Newton's method as suggested by Taflove [1], must be employed. Using this method, a plot (see Fig. (14)) of normalised phase velocity v_p/c for a numerical wave propagating in a vacuum has been calculated a function of propagation angle ϕ. The plot corresponds to the case $S = 0.5$ and $N_\lambda = 20$. This plot

Figure 14: Plot of normalised phase velocity as a function of propagation angle within the FDTD grid. Corresponds to the case $S = 0.5$ and $N_\lambda = 20$.

illustrates the general relationship between propagation angle and normalised phase velocity. Numerical dispersion may be reduced by increasing N_λ. Fig. (15) shows a plot of $1 - v_p/c$ for a numerical wave with $\phi = \pi/4$, $S = 0.5$ and increasing values of N_λ. The plot demonstrates that even at what is considered an impractical value for N_λ, there is still numerical dispersion.

Figure 15: Plot showing 1-v_p/c as a function of N_λ. Corresponds to case of $S = 0.5$ and $\phi = \pi/4$.

B.5 Numerical stability

The FDTD method is not unconditionally numerically stable. The time step must be bounded in order to maintain stability. Taflove [1] shows that the following relationship must hold in order for the scheme to remain numerically stable:

$$0 \leq c\Delta t \sqrt{\frac{1}{\Delta_x^2} + \frac{1}{\Delta_y^2} + \frac{1}{\Delta_z^2}} \leq 1 \tag{67}$$

where c is the speed of light in the fastest region of the computational space. In the special case of a cubic grid in three dimensions this reduces down to the simple case:

$$\Delta t \leq \frac{\Delta}{c\sqrt{3}} \tag{68}$$

B.6 Selection of grid resolution

The size of the Yee cell must be selected carefully to ensure the simulation is sufficiently accurate. Recall from Sec. (A.1) that central difference operations have an error of the order of the square of the distance between sample points. Thus supposing that Δ is the maximum of Δ_x, Δ_y and Δ_z, the error associated with each difference operation would be $O(\Delta^2)$. By looking at the derivation of this result it becomes evident that the central difference operation produces an exact result for quantities which vary linearly. Thus Δ should be chosen sufficiently small such that the waveforms vary approximately linearly between field component sample points on adjacent Yee cells. As a general rule, Δ is chosen to be no larger than $\lambda/20$.

Accuracy is however not the only factor which affects the choice of Δ. This is because all scattering objects must be built up using a staircase approximation. Thus, small features must be constructed using cuboids with sides of at least Δ in length. Thus the choice of Δ is determined not only by the need to accurately sample the field but also to accurately model the scatterer.

B.7 Absorbing boundary conditions

Scattering problems in optics generally involve a scatterer in an infinite space or infinite half space. Due to computers having only a finite amount of memory, the computational region must be truncated somehow using an approximate boundary condition which closely approximates an infinite boundary

condition. It is very difficult to devise such a boundary condition based solely upon Maxwell's equations in a difference method such as the FDTD method. This is because at the boundary of the computational space, not all difference operations can be evaluated because some data is missing, in particular those data points which would be outside the artificial boundary of the computational domain. A boundary condition of this type is called an Absorbing Boundary Condition (ABC).

ABCs result in a boundary condition with an extremely low reflection of outgoing radiation. An ideal ABC would absorb all outgoing radiation without reflecting any back into the computational volume. In practice there is always a small reflection however as long as the reflection is sufficiently small the ABC will not be the factor limiting the simulation accuracy.

The first generations of absorbing boundary conditions were all what are known as analytic ABCs. These have largely been made redundant due to the development of the Perfectly Matched Layer (PML) which will be discussed later in this section. Analytic ABCs either try to calculate the difference operations which cannot be evaluated due to missing data at the computational space boundary or use an alternative difference scheme at the boundary. For example, radiation operators [17, 18, 19, 20] provide a means for estimating the derivative of a propagating wave in the direction of propagation based upon spatial derivatives transverse to the direction of propagation and temporal derivatives. This provides a way to approximate the derivatives which otherwise could not be calculated because of missing data. Another class of analytic ABCs use what is known as a one-way wave equation [21, 9, 22] to devise an alternative differencing scheme to be applied at the boundary of the computational region. A one-way wave equation is a wave equation which permits propagation of a wave in one direction only. The final class of analytic ABCs uses a scheme to extrapolate from historical data the field at the missing data points [1]. This draws upon the principle of retarded radiation so that data from an earlier time is used to calculate the field at a later time at points located further from the scatterer than the initial points. These methods have been used to good effect over a period of decades. The PML has now superseded them in most applications. The theory behind the PML will be discussed now.

The previously introduced analytic ABCs all use different update equations on the boundary of the computational space. The PML operates in quite a different manner. A PML is a layer of absorbing material placed between the scatterer and a PEC boundary which terminates the computational space. The material is designed such that it has, in principle, zero reflection for plane

waves of any frequency propagating at arbitrary angle of incidence relative to the PML boundary. The absorbing nature of the PML causes waves which propagate through it to be attenuated such that there is very little energy reflected back of the PEC boundary. As long as the PML is situated in the scattered field region of the FDTD computational space it is very useful for simulating open region scattering problems.

The PML was first introduced in two dimensions by Berenger [10] and then later in three dimensions [23]. Berenger's formulation employs a non-physical modification of Maxwell's equations. For brevity a full derivation of Berenger's PML will not be presented but the salient details will be. To understand how such a material may be constructed, consider a plane wave incident normally upon an interface between two materials as shown in Fig. (16). Using Fresnel's equations it may be shown that to eliminate the reflected wave ($\mathbf{E}_r$ and $\mathbf{H}_r$), the following relationship must hold:

$$\mu_1^* k_0 n_2 = \mu_2^* k_0 n_1 \tag{69}$$

where k_0 is the wave number in material 1, $\mu_1^* = \mu_{r1}\mu_0$, $\mu_2^* = \mu_{r1}\mu_0(1 - \sigma_2^*/\imath\omega_0\mu_{r2}\mu_0)$, $n_2 = \sqrt{\mu_2^*\epsilon_2^*}/\sqrt{\epsilon_0\mu_0}$, $n_1 = \sqrt{\mu_1^*\epsilon_1^*}/\sqrt{\epsilon_0\mu_0}$, $\epsilon_2^* = \epsilon_{r2}\epsilon_0(1-\sigma_2/(\imath\omega_0\epsilon_{r2}\epsilon_0)$, $\epsilon_1^* = \epsilon_{r1}\epsilon_0$ and ω_0 is the angular frequency of the time harmonic plane wave. Some manipulations show that Eq. (69) requires that $\sqrt{\epsilon_1^*/\mu_1^*} = \sqrt{\epsilon_2^*/\mu_2^*}$.

Figure 16: Figure showing a plane wave normally incident upon an interface between a dielectric and a conducting material.

This in turn requires that $\epsilon_{r2}/\epsilon_{r1} = \mu_{r2}/\mu_{r1}$ and $\sigma_2^*/\mu_{r1} = \sigma_2/\epsilon_{r1}$. This provides the basis for a material interface between a dielectric region and an absorbing region with zero reflection. This is however only valid at normal incidence.

In order to derive an absorbing material with a reflectionless interface with dielectric materials at oblique incidence, Berenger introduced a so called splitting of Maxwell's equations. Each field component is split into two sub components, for example $E_x = E_{xy} + E_{xz}$. Using this splitting each of Eqs. (45) to (50) may be rewritten to form a new set of coupled differential equa-

tions:

$$\frac{\partial H_{xz}}{\partial t} = \frac{1}{\mu_r \mu_0}\left[\frac{\partial (E_{yx}+E_{yz})}{\partial z} - \sigma_z^* H_{xz}\right] \quad (70)$$

$$\frac{\partial H_{xy}}{\partial t} = \frac{1}{\mu_r \mu_0}\left[-\frac{\partial (E_{zx}+E_{zy})}{\partial y} - \sigma_y^* H_{xy}\right] \quad (71)$$

$$\frac{\partial H_{yx}}{\partial t} = \frac{1}{\mu_r \mu_0}\left[\frac{\partial (E_{zy}+E_{zx})}{\partial x} - \sigma_x^* H_{yx}\right] \quad (72)$$

$$\frac{\partial H_{yz}}{\partial t} = \frac{1}{\mu_r \mu_0}\left[-\frac{\partial (E_{xy}+E_{xz})}{\partial z} - \sigma_z^* H_{yz}\right] \quad (73)$$

$$\frac{\partial H_{zx}}{\partial t} = \frac{1}{\mu_r \mu_0}\left[-\frac{\partial (E_{yx}+E_{yz})}{\partial x} - \sigma_x^* H_{zx}\right] \quad (74)$$

$$\frac{\partial H_{zy}}{\partial t} = \frac{1}{\mu_r \mu_0}\left[\frac{\partial (E_{xy}+E_{xz})}{\partial y} - \sigma_y^* H_{zy}\right] \quad (75)$$

$$\frac{\partial E_{xy}}{\partial t} = \frac{1}{\epsilon_r \epsilon_0}\left[\frac{\partial (H_{zx}+H_{zy})}{\partial y} - \sigma_y E_{xy}\right] \quad (76)$$

$$\frac{\partial E_{xz}}{\partial t} = \frac{1}{\epsilon_r \epsilon_0}\left[-\frac{\partial (H_{yx}+H_{yz})}{\partial z} - \sigma_z E_{xz}\right] \quad (77)$$

$$\frac{\partial E_{yx}}{\partial t} = \frac{1}{\epsilon_r \epsilon_0}\left[-\frac{\partial (H_{zx}+H_{zy})}{\partial x} - \sigma_x E_{yx})\right] \quad (78)$$

$$\frac{\partial E_{yz}}{\partial t} = \frac{1}{\epsilon_r \epsilon_0}\left[\frac{\partial (H_{xy}+H_{xz})}{\partial z} - \sigma_z E_{yz}\right] \quad (79)$$

$$\frac{\partial E_{zx}}{\partial t} = \frac{1}{\epsilon_r \epsilon_0}\left[\frac{\partial (H_{yx}+H_{yz})}{\partial x} - \sigma_x E_{zx}\right] \quad (80)$$

$$\frac{\partial E_{zy}}{\partial t} = \frac{1}{\epsilon_r \epsilon_0}\left[-\frac{\partial (H_{xy}+H_{xz})}{\partial y} - \sigma_y E_{zy}\right] \quad (81)$$

where it has been assumed that the PML is a source free region and $(\sigma_x, \sigma_y, \sigma_z)$ and $(\sigma_x^*, \sigma_y^*, \sigma_z^*)$ are analogous to electric and equivalent magnetic losses respectively. It is interesting to note that if $\sigma_x = \sigma_y = \sigma_z = \sigma_x^* = \sigma_y^* = \sigma_z^* = 0$ then the above set of differential equations yield Maxwell's equations in a lossless. Berenger showed that by making (σ_x, σ_x^*) non zero, a material attenuates a wave propagating with a wave vector component in the x-direction and similarly for (σ_y, σ_y^*) and (σ_z, σ_z^*). Furthermore, the material will be reflectionless for a plane wave incident at any angle. Thus in order to surround a scatterer in such a way that outgoing radiation is not reflected back to the scatterer, the PML must be constructed as shown in Fig. (17). It is then a simple matter to develop the update equations for the split formulation in a manner very similar to the original Yee case. It should be mentioned that the

Figure 17: Diagram showing the various material regions used in the top right hand corner of a PML [23].

PML update equations employ exponential time stepping [24]. Exponential time stepping is especially designed to be used within materials of high conductivity and better models the exponentially decaying fields present within such materials. The update equations may be found in Berenger [23] and Taflove [1].

Although in the continuous case the PML results in zero reflection of outgoing radiation this is not the case in the discretised version actually used in the FDTD. A numerical reflection results from discretisation of the PML equations. In order to minimise the numerical reflection, the electrical and equivalent magnetic loss are increased smoothly from a minimum at the interface between free space and PML up to a maximum at the PEC boundary. Another source of reflection is the PEC boundary itself. Although the PML is designed to attenuate the field there will still be some radiation reflected back. Berenger showed that for a conductivity profile of $\sigma(\rho)$ and PML thickness δ that the maximum reflection coefficient for a wave propagating into PML, reflecting off the PEC boundary and then back through the PML again is:

$$R = \exp\left(-\frac{2}{\epsilon_0 c}\int_0^{\delta}\sigma(\rho)d\rho\right) \tag{82}$$

In practice a conductivity profile of the form [25] $\sigma(\rho) = \sigma_m(\rho/\delta)^n$ is used for some integer n and constants σ_m and δ. These parameters are chosen to ensure a suitable upper bound on the reflection coefficient.

Although it is extremely effective, it is slightly dissatisfying to use a modified set of Maxwell's equations without physical justification. Fortunately, it has been shown that the split formulation is equivalent to two other interpretations of the PML. One interpretation considers the PML as an anisotropic absorber. In this case the material properties are described using tensors. The makeup of each tensor is different for each region within the PML as depicted in Fig. (82). This interpretation was first introduced by Sacks *et al.* [26] in the context of the FEM. The other interpretation considers the PML as a material in a so called stretched coordinate system defined by Maxwell's equations with the standard ∇ operator replaced by $\nabla_s = \hat{\mathbf{x}}\frac{1}{s_x}\frac{\partial}{\partial x} + \hat{\mathbf{y}}\frac{1}{s_y}\frac{\partial}{\partial y} + \hat{\mathbf{z}}\frac{1}{s_z}\frac{\partial}{\partial z}$ [27] where the x-, y- and z-axes are stretched by factors s_x, s_y and s_z respectively. It may be shown that by making these factors complex that waves may be attenuated in a manner equivalent to the preceding two interpreta-

tions of the PML. These two additional interpretations have been included for completeness but as the split formulation was implemented, they will not be discussed in detail here.

One point which should be noted is that it has been shown that PMLs do not attenuate evanescent waves [28, 29, 30]. The only attenuation which occurs is due to the attenuation inherent to evanescent waves. There is also a numerical reflection at the PML interface. The conclusion of this work is that when a PML is employed it should ideally be situated sufficiently far from a scatterer so that evanescent waves have attenuated significantly. If this is not possible then the PML may need to be made thicker than usual.

B.8 Subtle aspects of the FDTD method

This section discusses aspects of the FDTD method which are typically not mentioned in the literature. They are however problems which may adversely affect the performance of the FDTD method if not properly handled.

B.8.1 Interpolation

Whilst the FDTD method solves for both the electric and magnetic fields concurrently, each field component is evaluated at a different point in space. It is thus necessary to use interpolation in order to evaluate the electric and magnetic field vectors at common sample points. To see how this might be done, suppose that the electric and magnetic field vectors are to be calculated at position $(i + 1/2, j - 1/2, k - 1/2)$ in the Yee cell of Fig. (18) which is indicated by a dot in the Yee cell. The field sample points of the Yee cells in close proximity to the reference point along with the reference point itself are shown above the Yee cell for clarity. For the case of the electric field a simple application of linear interpolation between adjacent sample points is required to find the field at the reference position. Finding the magnetic field components is more difficult however. This involves performing three separate interpolations. For example, consider the diagram in Fig. (18) showing four adjacent H_z sample points. In order to find H_z at the reference point, H_z^{i1} and H_z^{i2} must be found using linear interpolation. Then the field at the reference point is found by interpolation between H_z^{i1} and H_z^{i2}

The problem with this scheme is that linear interpolation is not very accurate. For example, consider a 1-dimensional travelling scalar wave of the form $y(x,t) = \sin(kx - \omega t)$ and assume that the wave is sampled spa-

Figure 18: Diagram indicating how interpolation is used to calculate the electric and magnetic field at a common reference point.

tially at $x = 0$ and $x = \Delta = 2\pi/(Nk)$ where N is the number of sample points per wavelength. Suppose that at each instant in time linear interpolation is used to find the value of the wave at $x = \Delta/2$. This would yield $y(x,t) = \cos(\pi/N)\sin(\pi/N - \omega t)$ which has the correct phase but incorrect amplitude. The percentage error in the amplitude is plotted in Fig. (19). The plot shows that the error is significant even at $N = 20$ and is thus not accurate enough to be used in the FDTD simulation. Fortunately, away from scattering objects the fields vary quite smoothly. This means that simple high order interpolation scheme may be employed.

Figure 19: Plots showing percentage amplitude error for linear and cubic interpolation of a travelling wave.

Cubic interpolation is such a higher order scheme that requires four data points in order to perform interpolation. It is easy to show that when the value of a function f is known at positions $(x_1, x_2, x_3, x_4) = (x_1, x_1 + \Delta, x_1 + 2\Delta, x_1 + 3\Delta)$ as shown in Fig. (20) then $f(x_2 + \Delta/2)$ may be found using cubic interpolation as:

$$f(x_2 + \Delta/2) = -1/16 f(x_1) + 9/16 f(x_2) + 9/16 f(x_3) - 1/16 f(x_4) \quad (83)$$

The amplitude error when cubic interpolation is employed for the travelling wave example is also shown in Fig. (19). This is at least an order of magnitude better than the linear case across all values of N.

Figure 20: Diagram showing the set of sample points required to use cubic interpolation.

Note that this requires that four field values are used to find each electric field value and 16 field values are required to find each magnetic field value. It is easy enough to see how this works for the electric field case as instead of taking two sample points along a line as in Fig. (18), four are taken. It is more complex in the case of the magnetic field components. Fig. (21)(a) shows how cubic interpolation is used five times to find the value of H_x at the reference point. Firstly the value of H_x is found at each point denoted with a hollow circle. These are found using cubic interpolation along the horizontal

line through each hollow circle. Then each of these interpolated values is in turn used to find the field at the reference point which is denoted by a solid dot. At the edges of the computational domain a slightly different method must be employed. Interpolation is still employed however the interpolated values may not be calculated in the centre of the sample points. This is illustrated in Fig. (21)(b).

Figure 21: Diagram showing how cubic interpolation is used to calculate the value H_x at a common reference point. (a) shows an example away from the edges of the computational domain whilst (b) shows an example at the edges of the computational domain.

B.8.2 Asymmetry

Implementation of the Yee algorithm exactly as is suggested by Taflove and Hagness [1] yields unnaturally asymmetric resultant fields. The origin of the asymmetry is easy to find by considering the diagram in Fig. (22) which shows a two-dimensional Transverse Electric (TE) FDTD grid. This corresponds to the case where the grid extends uniformly to infinity in the positive and negative z-directions. The central shaded cell has a different refractive index, n, to the two surrounding cells which are composed of free space. The centre of each cell is located where the H_z sample points are located.

Under the most basic FDTD scheme the material properties of a cell are determined by the material properties of the centre of the cell. All update equations for the cell then employ the material properties at the cell centre. Consider however a plane wave travelling in the positive z-direction linearly polarised in the x-direction. Then the update equation for E_{x1} uses refractive index n and the update equation for E_{x2} uses refractive index 1. This means that E_{x1} and E_{x2} must differ. This leads to asymmetry since these field components are equally spaced from the centre of the scattering cell and are symmetric with respect to the polarisation of the incident field and scattering object.

This problem arises because the use of a nearest neighbour approach to selecting the refractive index to use enforces a directionality upon the algorithm. This is overcome by interpolating the material properties from the cell origins to where the update equations are being updated. This eliminates the asymmetry in a rigorous manner.

Figure 22: Diagram showing two dimensional TE FDTD grid with a single scattering cell (shaded) with refractive index n.

B.9 Evaluation and analysis

B.9.1 Propagation of focused light

Tests were performed in order to gauge the accuracy of modelling a focused x-polarised beam using the FDTD method. This was done by introducing the focused beam into a homogeneous free space FDTD grid. The resulting field distribution was then compared to that obtained analytically using the Debye-Wolf integral. In each test, a single parameter was varied to see which parameters affect the simulation accuracy. The base test, to which all others are compared, is denoted test 'a'. Test 'a' had the following simulation parameters:

- $\lambda = 628.3$nm
- $\Delta_x = \Delta_y = \Delta_z = \lambda/20$
- I=200, J=200, K=100
- $\Delta t = 0.95\times$Courant
- $\Delta\lambda = 60$nm
- $NA = 0.92$

where λ is the wavelength of the focused beam, I, J and K are the number of Yee cells in the x-, y- and z-directions respectively. $\Delta\lambda$ is the spectral FWHM of the modulating Gaussian pulse and Δt is the time step employed in the FDTD method, set to 0.95 of the limit imposed by the Courant stability criteria (see Eq. (68)). The focused beam is introduced to the FDTD grid very close to its waist, normally incident upon the lateral (xy) plane of the FDTD grid. The position $z = 0$ in the FDTD simulation space corresponds to the focus of the beam. The size of the grid in the z-direction or, equivalently, K was varied where necessary in order to fit the simulation into the computer memory available.

The accuracy of each simulation is measured using a metric which may be described as an aggregate error measure. It is calculated according to:

$$\epsilon_{\mathbf{E}}^{\mathbf{s}}(z) = \frac{\sum_{i=1}^{I}\sum_{j=1}^{J}\sum_{k=1}^{\text{floor}(z/\Delta_z)} \left|\left(\mathbf{E}^{\text{FDTD}}(i,j,k) - \mathbf{E}^{\text{Analytic}}(i,j,k)\right)\cdot\mathbf{s}\right|^2}{\sum_{i=1}^{I}\sum_{j=1}^{J}\sum_{k=1}^{\text{floor}(z/\Delta_z)} \left|\mathbf{E}^{\text{Analytic}}(i,j,k)\cdot\mathbf{s}\right|^2} \tag{84}$$

where it is understood that $\mathbf{E}(i,j,k)$ refers to the field at position $\mathbf{E}(i\Delta_x, j\Delta_y, k\Delta_z)$ and $\mathbf{s}$ is a vector in the direction that the error is to be calculated in. The component-wise aggregate errors $\epsilon_{\mathbf{E}}^{\hat{\mathbf{i}}}$, $\epsilon_{\mathbf{E}}^{\hat{\mathbf{j}}}$ and $\epsilon_{\mathbf{E}}^{\hat{\mathbf{k}}}$ where $\hat{\mathbf{i}}$, $\hat{\mathbf{j}}$ and $\hat{\mathbf{k}}$ are the unit vectors of the Cartesian coordinate system have been plotted in Fig. (23). Each plot has 6 lines on it corresponding to each test. The tests are labelled 'a' to 'f' and the parameters used for each test are outlined in Table 2.

test	λ/Δ_x	λ/Δ_y	λ/Δ_z	I	J	K	$\Delta\lambda$
a	20	20	20	200	200	100	60nm
b	20	20	20	**220**	**220**	100	60nm
c	**22**	**22**	**22**	200	200	90	60nm
d	20	20	20	200	200	100	**50nm**
e	20	20	20	**240**	**240**	80	60nm
f	**25**	**25**	**25**	200	200	70	60nm

Table 2: Table showing the parameters used in each of the FDTD simulations. Test a is the base case and all subsequent tests vary only a single parameter. The parameters which are changed are in bold.

Figure 23: Aggregate error for each of the electric field components for simulations a to c. Note that the error for test a is obscured by the line for test d since they have such similar errors.

The base test, 'a', produced accurate results with the aggregate error of the x-component remaining below 1% several wavelengths down the grid. The error in the y-component is higher than in the x- and z-components. This is most likely because the y-component is functionally more complex than the x and z and it also has a lower magnitude. This is demonstrated in Fig. (24) where the magnitude of the electric field components of the particular in-focus beam is illustrated.

Figure 24: Illustrations of the magnitude of each component of the electric field for an in focus x-polarised beam with NA 0.92.

Test 'b' employed a wider lateral grid size and resulted in a reduction in the aggregate error for all components. Test 'e' used an even wider grid and resulted in a further reduction in the aggregate error for all components. This demonstrates that the most significant parameter is the lateral width of the FDTD grid.

The other tests show that there is little benefit to be gained, as far as this example is concerned, in using smaller values of Δ_x, Δ_y, Δ_z and $\Delta\lambda$. The conclusion of these tests is that the FDTD grid should be chosen to be as wide in the lateral directions as possible. Given that the main constraint involved with performing FDTD calculations is computer memory, all other parameters should be set to allow the size of the lateral grid to be maximised.

B.9.2 Scattering by a sphere

One of the most commonly used test cases for gauging the accuracy of FDTD scattering calculations is scattering by a sphere. This is because the solution is given analytically by the series of Mie. In this section, the accuracy of the calculation of the scattered field was measured for a range of sphere relative permittivities, denoted ϵ_r, and conductivities, denoted σ. It is assumed that a plane wave of wavelength $\lambda = 405$nm, propagating along the positive z-axis and polarised in the x-direction is incident upon a sphere of radius $\lambda/2$ situated in a vacuum. The scattered field was calculated on a cuboid surface positioned asymmetrically with respect to the sphere, as illustrated in Fig. (25). This was done because the FDTD calculation required too much memory to calculate the scattered field in the entire volume. By positioning the surface asymmetrically, both near and intermediate fields could be assessed.

In the case of the FDTD method, two calculations were required for each sphere type. This is because the incident field was calculated in a separate FDTD calculation and subtracted from the result obtained with a sphere present to yield the scattered field. Because of numerical dispersion, this is more accurate than subtracting the analytically calculated incident field. The squared magnitudes for each field component for a sphere of relative permittivity 2, calculated using both Mie and FDTD methods are shown in Fig. (26). The fields appear to be very similar purely from a visual inspection. In order to study the error more rigorously, it is necessary to introduce an

Figure 25: Diagram illustrating the position of the scattering sphere and the surface where the field is calculated which is represented by the extremities of the axes. The staircasing approximation to the sphere is illustrated in the inset image of the sphere.

aggregate error measure similar to that used in Sec. (B.9.1). Here, it is

Figure 26: The squared magnitude of each electric field component of field scattered by a dielectric sphere of relative permittivity 2 as calculated using the FDTD method (top) and Mie series (lower).

defined as:

$$\epsilon_{\mathbf{E}}^{\mathbf{s}} = \frac{\sum_{i=1}^{i=N_{vertices}} \left| \left(\mathbf{E}_i^{\mathrm{FDTD}} - \mathbf{E}_i^{\mathrm{Mie}} \right) \cdot \mathbf{s} \right|^2}{\sum_{i=1}^{i=N_{vertices}} \left| \mathbf{E}_i^{\mathrm{Mie}} \cdot \mathbf{s} \right|^2} \tag{85}$$

where $N_{vertices}$ is the number of vertices on the surface where the field is calculated and $\mathbf{E}_i$ is the electric field at vertex i (could be either FDTD or Mie). $\mathbf{s}$ is a vector in the direction in which the field's accuracy is to be measured. Fig. (27) shows the aggregate error for the x-, y- and z-field components as a function of the relative permitivity of the sphere. Note that the conductivity was set to 0 for this simulation. This shows that the error in the x- and z-components remains below %1 for relative permitivities upto approximately 3.5. There is a larger error in the y-component but it is still acceptable given that its magnitude is much less than that of the x- and z-components. This is a good result because the common type of dielectrics (such as plastic and latex) have a refractive index yielding a relative permitivity of less than 3.5. The plot of aggregate error for the x-, y- and z-field components as a func-

Figure 27: Plots showing the aggregate error for each electric field component as a function of the relative permitivity of the sphere.

tion of conductivity is shown in Fig. (28). Note that the relative permitivity was set to 1 for this simulation. This plot shows that the error becomes

unacceptably high for conductivities greater than approximately $10^5(S/m)$. This is because for higher conductivities the field decays so rapidly within the sphere that it cannot be accurately modelled by the FDTD's difference equations. This is a well known phenomenon in the field of FDTD modelling (see for example Refs. [31, 32]). It is also known that at high conductivities, approximation of objects by staircasing becomes less accurate [33]. There are thus two problems here. The first is how to more accurately model metals. Much work has been done on this and the most common approach is to incorporate a dispersive material model into the FDTD method (see for example Refs. [34, 35]. This also entails using a very fine FDTD grid and can lead to substantial memory consumption.

Much work has also been done on the problem of staircasing. In general, however, each method makes the FDTD substantially more complex for only a moderate improvement in accuracy. Furthermore, the improvement is usually only useful in a restricted range of problems.

Figure 28: Plots showing the aggregate error for each electric field component as a function of the conductivity of the sphere.

B.10 Conclusions

This chapter introduced the well established FDTD method. It was shown that focused beams may be modelled accurately by employing a grid which is large in the lateral direction. It was shown that the grid should be as wide as possible. It was shown, however, that a width of ten wavelengths provides sufficient accuracy. It was also shown that a spectral width of the modulating Gaussian pulse should be in the range of 0.1 of the wavelength of the light source. It was also shown that a grid resolution of 20 samples per wavelengths provides sufficient accuracy. This work has not previously been published and should thus be considered original work.

The accuracy of the FDTD method, when applied to scattering problems, was also tested. It was shown that in the case of scattering by a dielectric sphere, the FDTD method remains accurate for realistic values of refractive index, say up to 2. In the case of a conducting sphere the FDTD becomes inaccurate at the modest conductivity of 10^6 S/m when using simulation parameters which would be used when simulating focused beams.